

From parameter space constraints to the precision determination of the leptonic Dirac CP phase

P. HUBER^a, M. LINDNER^b, W. WINTER^c

^a*Department of Physics, University of Wisconsin,
1150 University Avenue, Madison, WI 53706, USA*

^b*Physik-Department, Technische Universität München,
James-Franck-Strasse, 85748 Garching, Germany*

^c*School of Natural Sciences, Institute for Advanced Study,
Einstein Drive, Princeton, NJ 08540, USA*

June 27, 2018

Abstract

We discuss the precision determination of the leptonic Dirac CP phase δ_{CP} in neutrino oscillation experiments, where we apply the concept of “CP coverage”. We demonstrate that this approach carries more information than a conventional CP violation measurement, since it also describes the exclusion of parameter regions. This will be very useful for next-generation long baseline experiments where for sizable $\sin^2 2\theta_{13}$ first constraints on δ_{CP} can be obtained. As the most sophisticated experimental setup, we analyze neutrino factories, where we illustrate the major difficulties in their analysis. In addition, we compare their potential to the one of superbeam upgrades and next-generation experiments, which also includes a discussion of synergy effects. We find a strong dependence on the yet unknown true values of $\sin^2 2\theta_{13}$ and δ_{CP} , as well as a strong, non-Gaussian dependence on the confidence level. A systematic understanding of the complicated parameter dependence will be given. In addition, it is shown that comparisons of experiments and synergy discussions do in general not allow for an unbiased judgment if they are only performed at selected points in parameter space. Therefore, we present our results in dependence of the yet unknown true values of $\sin^2 2\theta_{13}$ and δ_{CP} . Finally we show that for δ_{CP} precision measurements there exist simple strategies including superbeams, reactor experiments, superbeam upgrades, and neutrino factories, where the crucial discriminator is $\sin^2 2\theta_{13} \sim 10^{-2}$.

^aEmail: phuber@physics.wisc.edu

^bEmail: lindner@ph.tum.de

^cEmail: winter@ias.edu

1 Introduction

After the measurements of the leading atmospheric and solar oscillation parameters (see, *e.g.* Ref. [1] and references therein), the most important task for the next generation neutrino oscillation experiments will be the search for a finite value of θ_{13} . Future reactor experiments [2], conventional beam experiments [3–5], or superbeams [6, 7] could establish $\sin^2 2\theta_{13} > 0$ for $\sin^2 2\theta_{13} \gtrsim 10^{-2}$. For smaller values of θ_{13} , superbeam upgrades (such as T2HK [6]) and β -beams [8, 9], or neutrino factories [10–12] continue the hunt. Once $\sin^2 2\theta_{13} > 0$ is established, it is possible to address the mass hierarchy and the value of δ_{CP} . In this study we discuss precision measurements of the leptonic Dirac CP phase as the most challenging task for neutrino oscillation physics within the framework of three-flavor neutrino oscillations.

The determination of the leptonic CP phase δ_{CP} has so far been discussed in different ways [8, 9, 13–65]. Some of them are CP violation measurements, which address the question if a CP violating value of δ_{CP} can be distinguished from the CP conserving values 0 and π . The sensitivity to maximal CP violation $\delta_{\text{CP}} = \pi/2$ or $\delta_{\text{CP}} = 3/2\pi$ has also been extensively studied. Another class are precision measurements of δ_{CP} , which have been investigated *e.g.* in the context of superbeam upgrades and neutrino factories. Many results are given only at some discrete points in parameter space and from this it is not possible to judge the overall performance of the considered setup. A discussion of the changes in the precision as function of the relevant parameter values is missing in most cases. The aim of this study is therefore to investigate the reason for differences in previous studies and to find a systematic way for comparing and classifying the CP sensitivities. We will demonstrate that these differences are indeed consistent, and we will illustrate how one can understand the underlying parameter dependence. In particular, we will find that the topology of the neutrino factory parameter space for small values of $\sin^2 2\theta_{13}$ is rather complicated.

From the theoretical point of view any value of δ_{CP} could be realized by nature, *i.e.* $\delta_{\text{CP}} \in [0, 2\pi[$. This means, for example, that sensitivity to maximal CP violation ($\delta_{\text{CP}} = \pi/2$ or $3/2\pi$) does very likely not correspond to the real world. In particular, the era of superbeams and reactor experiments within the next ten years will not be able to measure CP violation even under very optimistic assumptions [63]. Nevertheless, superbeams could exclude some values of δ_{CP} , and thus could restrict the possible parameter space. On the other end, at the high precision frontier, the investigation of CP violation might be too restrictive, since these future experiments could not only establish CP violation, but also constrain the parameter space for δ_{CP} even further. Therefore, all available information on δ_{CP} should be used, which then can be used for the optimization of future experiments, as input for neutrino mass models, or as motivation to continue hunting for leptonic CP violation.

One of the major difficulties in the analysis of future neutrino oscillation experiments is the huge number of parameters: In general, one has six simulated parameters (within their currently allowed ranges) and six fitted parameters, *i.e.*, a 12-dimensional parameter space. A performance indicator which condenses the information is therefore required in order to show the results as a function of the most relevant impact parameters. Such a performance indicator can, furthermore, be used for the comparison of experiments, for risk minimization with respect to the yet unknown parameter values, for the optimization of experiments, or

for the discussion of synergy effects. In this study, we use the “CP coverage” [45] as performance indicator for CP precision measurements. CP coverage is defined as the combined range of all fit values which fit the chosen simulated value of δ_{CP} .¹ Thus, a very small CP coverage corresponds to a good precision of δ_{CP} , whereas a CP coverage of 360° corresponds to no information on δ_{CP} . Note that this definition includes the case of disjoint regions (degeneracies) irrespectively of the precision within each individual region. For example, a value of 300° means that in total 60° of the possible parameter range of 360° can be excluded. Therefore, the CP coverage is a useful performance indicator which interpolates between exclusion measurements and high precision measurements of the leptonic Dirac CP phase. Note that the CP coverage should not be confused with the often used “CP fraction” (for example, in Ref. [66]). CP coverage refers to a range of fitted values of δ_{CP} , whereas CP fraction refers to a range of simulated/true values.

This study is organized as follows: In Section 2, we give a short introduction to three-flavor neutrino oscillations and the appearance channel in future long-baseline experiments. This section can be skipped by a reader familiar with the subject. Then we describe in Section 3 the analysis methods, where we only quickly repeat the general techniques described in earlier works, and rather extensively illustrate the problems connected with the analysis of future high precision instruments. This section is kept on a rather illustrative level, but is mandatory to understand the more technical details in Section 4. The quite general first part of Section 4 introduces performance indicators to differentiate experiment classes and to investigate synergies and shows the consequences for the physics potential of different experiments. The more technical second part of this section investigates the specific characteristics of superbeam and neutrino factory parameter space. The latter is not a prerequisite to understand Section 5, which discusses possible synergies among experiment types for future δ_{CP} precision measurements. In particular, it is a major objective of this section to investigate the complete parameter space in a systematized manner. Finally, we summarize our results in Section 6.

2 Neutrino oscillation framework

For long-baseline beam experiments, the electron or muon neutrino appearance probability P_{app} in matter carries the main information for CP effects. It can be expanded in the small hierarchy parameter $\alpha \equiv \Delta m_{21}^2/\Delta m_{31}^2$ and the small $\sin 2\theta_{13}$ up to the second order

¹In this study, we use always degrees for the CP coverage (fit values), whereas we use radians for simulated/true values of δ_{CP} .

as [31, 67, 68]:

$$\begin{aligned}
P_{\text{app}} &\simeq \sin^2 2\theta_{13} \sin^2 \theta_{23} \frac{\sin^2[(1 - \hat{A})\Delta]}{(1 - \hat{A})^2} \\
&\pm \alpha \sin 2\theta_{13} \sin 2\theta_{12} \sin 2\theta_{23} \sin \delta_{\text{CP}} \sin(\Delta) \frac{\sin(\hat{A}\Delta)}{\hat{A}} \frac{\sin[(1 - \hat{A})\Delta]}{(1 - \hat{A})} \\
&+ \alpha \sin 2\theta_{13} \sin 2\theta_{12} \sin 2\theta_{23} \cos \delta_{\text{CP}} \cos(\Delta) \frac{\sin(\hat{A}\Delta)}{\hat{A}} \frac{\sin[(1 - \hat{A})\Delta]}{(1 - \hat{A})} \\
&+ \alpha^2 \cos^2 \theta_{23} \sin^2 2\theta_{12} \frac{\sin^2(\hat{A}\Delta)}{\hat{A}^2}. \tag{1}
\end{aligned}$$

Here $\Delta \equiv \Delta m_{31}^2 L / (4E)$ and $\hat{A} \equiv \pm(2\sqrt{2}G_F n_e E) / \Delta m_{31}^2$ with G_F the Fermi coupling constant and n_e the electron density in matter. The sign of the second term is positive for $\nu_e \rightarrow \nu_\mu$ or $\nu_{\bar{\mu}} \rightarrow \nu_{\bar{e}}$ and negative for $\nu_\mu \rightarrow \nu_e$ or $\nu_{\bar{e}} \rightarrow \nu_{\bar{\mu}}$. The sign of \hat{A} is determined by the sign of Δm_{31}^2 and choosing neutrinos (factor +1) or antineutrinos (factor -1).

This expansion clearly identifies δ_{CP} as a genuine three-flavor effect in the second and third terms, which is double-suppressed by the mass hierarchy parameter α and $\sin 2\theta_{13}$. Since Δm_{21}^2 has turned out to be rather large within the LMA-allowed region [1, 69, 70], it became possible to determine δ_{CP} , but the bottleneck of any CP measurement will certainly be the true value of $\sin^2 2\theta_{13}$. So far, $\sin^2 2\theta_{13}$ has been only restricted to $\sin^2 2\theta_{13} \lesssim 10^{-1}$ by the CHOOZ and Palo Verde reactor data and recently also by the solar experiments [71]. If $\sin^2 2\theta_{13} > 0$ cannot be established by any experiment, then CP effects in neutrino oscillations can not be detected. As we will discuss later, for $\sin^2 2\theta_{13} > 0$, the actual value of $\sin^2 2\theta_{13}$ will determine the strategy to measure δ_{CP} .

In principle, the second term in Eq. (1) contains the intrinsic information on δ_{CP} close to the oscillation maximum, whereas the third term proportional to $\cos \delta_{\text{CP}} \cdot \cos \Delta$ is suppressed close to the oscillation maximum (where $\sin \Delta \sim 1$). In particular, it is easy to see that the probability difference $|P_{e\mu} - P_{\bar{e}\bar{\mu}}|$ (or $|P_{\mu e} - P_{\bar{\mu}\bar{e}}|$) in vacuum is just twice the second term in Eq. (1), which is often called ‘‘CP-odd probability difference’’. Therefore, it is well known that using both neutrinos and antineutrinos helps to extract the leptonic CP phase from Eq. (1). However, matter effects enhance the neutrino channel and suppress the antineutrino channel (for a normal mass hierarchy). In addition, a direct measurement of $|P_{e\mu} - P_{\bar{e}\bar{\mu}}|$ is not possible, since in an actual experiment only the convolution of the probability, the flux, the cross sections, and detector efficiencies is measured. Each part of this convolution may give rise to additional contributions to the ‘probability difference’, especially cross sections and efficiencies might prove to make the use of a mere ‘probability difference’ pointless. Furthermore, the appearance event rates are proportional to the full Eq. (1). Therefore, matter effects, matter density uncertainties, and the complicated parameter dependence in Eq. (1) spoil the clean extraction of δ_{CP} . In particular, the complicated parameter dependence of the oscillation probability leads to correlations with $\sin^2 2\theta_{13}$ [31, 37] and multi-parameter correlations [45], as well as to the $(\delta_{\text{CP}}, \theta_{13})$ [37], $\text{sgn}(\Delta m_{31}^2)$ [72], and $(\theta_{23}, \pi/2 - \theta_{23})$ [73] degeneracies, *i.e.*, an overall ‘‘eight-fold’’ degeneracy [35]. In the analysis, we will take into account all of these degeneracies. Note however, that the $(\theta_{23}, \pi/2 - \theta_{23})$

degeneracy is not present, since we always adopt for the true value of θ_{23} the current atmospheric best-fit value $\theta_{23} = \pi/4$. Hence, we will effectively deal with a “four-fold” degeneracy.

From the theoretical point of view, the second term in Eq. (1) is especially interesting for CP violation measurements, since the CP violating effects are proportional to $\sin \delta_{\text{CP}}$. However, only using information close to the oscillation maximum, *i.e.*, the $\sin \delta_{\text{CP}}$ -term, leaves an intrinsic ambiguity between δ_{CP} and $\pi - \delta_{\text{CP}}$. This ambiguity can be resolved with the $\cos \delta_{\text{CP}}$ -term, as well as this term helps to disentangle δ_{CP} from $\sin^2 2\theta_{13}$. This means that for CP precision measurements a contribution of this term is favorable. For example, neutrino factories usually operate quite far off the oscillation maximum, which means that there is some contribution of the $\cos \delta_{\text{CP}}$ -term anyway. Note that for an experiment where the $\sin \delta_{\text{CP}}$ -term dominates, one naturally expects a strong dependence of the CP precision on the true value of δ_{CP} itself. In the high statistics dominated regime, the CP precision should be best close to 0 and π , since the derivative of $\sin \delta_{\text{CP}}$ is largest there, and worst to $\pi/2$ and $3/2\pi$. This, of course, can be changed by systematics and other effects.

Another interesting feature in Eq. (1) is the condition $\sin(\hat{A}\Delta) = 0$ (not to mix up with $\hat{A} = 1$, which is the matter resonance condition). It makes all but the first term in Eq. (1) disappear and thus allows a clean measurement of $\sin^2 2\theta_{13}$ and the sign of Δm_{31}^2 without correlations with the CP phase [35, 74]. This “magic baseline” [55, 75] condition is, for the first non-trivial solution, equivalent with $\sqrt{2}G_F n_e L = 2\pi$ or, depending on the assumptions, $L \sim 7500$ km. Its strength is the independence of all oscillation parameters, thus its value is known *a priori*. In combination with a shorter baseline, it can be also very efficient to access CP effects by resolving the intrinsic correlations and degeneracies [55]. We will show the obtainable precision using this option, later on.

For the oscillation parameters, we use, if not stated otherwise, $\Delta m_{31}^2 = 2.5 \cdot 10^{-3} \text{ eV}^2$, $\sin^2 2\theta_{23} = 1$, $\Delta m_{21}^2 = 7.0 \cdot 10^{-5} \text{ eV}^2$, and $\sin^2 2\theta_{12} = 0.8$. The numbers are similar to the ones from Refs. [71, 76].² In addition, we assume a normal mass hierarchy, since it turns out that, though there are quantitative differences, the assumption of an inverted mass hierarchy does not produce excitingly new effects in CP measurements [46]. We only use values for $\sin^2 2\theta_{13}$ below the current bound $\sin^2 2\theta_{13} \lesssim 0.1$ [71] and do not make any special assumptions about δ_{CP} . However, we will show in some cases the results for chosen selected values of δ_{CP} .

3 Analysis methods

We now describe briefly the general analysis methods, the used experiments and the computation of the CP coverage, which has to be done in an efficient way. In particular, the topology of the neutrino factory parameter space including the $(\delta_{\text{CP}}, \theta_{13})$ -degeneracy makes the computation of the CP coverage for very small values of $\sin^2 2\theta_{13}$, *i.e.*, a relatively flat

²However, the latest KamLAND results suggest a slightly higher value for Δm_{21}^2 [1, 69, 70], which were released after the calculations for this study have been performed (the overall calculation time was about three months). Since the CP effects are larger for larger values of Δm_{21}^2 , our results can be understood as the conservative limit.

topology, quite complicated.³ Thus we will demonstrate how the CP coverage, which is a highly condensed performance indicator, is obtained from the (marginalized) $\Delta\chi^2$, how the degeneracies are located, and what their effects are. Most of the shown examples in this section will be computed for a neutrino factory, since this experiment implies the highest level of sophistication.

3.1 The experiments and their simulation

In general, we use a three-flavor analysis of neutrino oscillations including matter effects. The matter density profile is taken to be constant with 5% uncertainty, to take into account matter density uncertainties as well as matter profile effects [59, 77, 78]. The analysis is performed with the $\Delta\chi^2$ method using the GLOBES software [79]. We take into account statistics, systematics, correlations, and degeneracies, where the correlations originate in the projection of the six-dimensional fit manifold onto the axis of the parameter of interest [45]. We use a local minimizer for this projection, which means that one has to be especially careful to find all degenerate solutions and not to miss any relevant local minimum. The correlations account for the fact that an experiment (or combination of experiments) cannot entirely resolve the intrinsic structure of the oscillation probabilities, but effectively measures a combination of the oscillation parameters. In principle, we assume that each experiment (or combination of experiments) will provide the best measurement of the leading atmospheric oscillation parameters at that time, which is coming from the disappearance channels of the accelerator-based experiments. For the solar parameters, we assume that the ongoing KamLAND experiment will improve the errors down to a level of about 10% on each Δm_{21}^2 and θ_{12} [80, 81].

The best precision is obtained for neutrino factories, where we will in most cases use the representative NuFact-II from Ref. [45]. In its standard configuration, it uses 4 MW target power ($5.3 \cdot 10^{20}$ useful muon decays per year), a baseline of 3 000 km, and a magnetized iron detector with a fiducial mass of 50 kt. We choose a symmetric operation with 4 yr in each polarity. For comparison and reference, we use the T2HK upgrade proposed in Ref. [6] with a target power of 4 MW, a baseline of 295 km, and a water Cherenkov detector with a fiducial mass of 1 000 kt [45]. It operates two years in the neutrino running mode, and six years in the antineutrino running mode to account for the lower antineutrino cross section.⁴ In addition, we compare in some cases with a scenario where we could be in ten years from now, which corresponds to the scenario “After ten years” from Ref. [63].⁵ It includes the two first-generation superbeams T2K [6] and NO ν A [7], where the simulation is described in Ref. [46] and the parameters used in Ref. [63]. In summary, both correspond very much to their standard scenarios as in the LOIs with a total running time of five years in the neutrino

³Note that this degeneracy may not only appear for the best-fit solution, but also in the $\text{sgn}(\Delta m_{31}^2)$ -degeneracy, leading (for maximal mixing) to a four-fold ambiguity.

⁴For the analysis of δ_{CP} , it turns out that in most cases the optimal performance can be reached for almost equal numbers of total events in the neutrino and antineutrino operation modes. Thus, if we assume given total running time, the fraction of the optimal antineutrino running time is primarily determined by the cross section ratio between neutrinos and antineutrinos [46].

⁵Here, we do not take into account the MINOS, ICARUS, and OPERA experiments, since their contribution to the final result would be marginal.

running mode for each experiment. However, for $\text{NO}\nu\text{A}$, we use a baseline of 812 km at an off-axis angle of 0.72° , a target power of 0.43 MW ($4.0 \cdot 10^{20}$ protons on target per year) and a low- Z -calorimeter as detector with a fiducial mass of 50 kt [66].⁶ In addition, the scenario uses the large reactor experiment **Reactor-II** introduced in Ref. [82] to disentangle θ_{13} and δ_{CP} ,⁷ which has a baseline of 1.7 km and an integrated luminosity of 8 000 t GW yr. We call the combined scenario **T2K+NO ν A+Reactor-II**.

The scenario **T2K+NO ν A+Reactor-II** is quite sophisticated, but it could be reached within ten years from now and it illustrates how fast and how much one could push for δ_{CP} within moderate time scales. Furthermore, we use **T2HK** as a very advanced superbeam upgrade to discuss what one could achieve within the superbeams era. Finally, and as the major part of this work, we investigate a standard scenario **NuFact-II** for neutrino factories, which might be the ultimate tool for δ_{CP} . A higher gamma β -beam may have a comparable potential and take this role if technically feasible, but this needs further study [83].

3.2 From $\Delta\chi^2$ to the CP coverage

The CP coverage presents the information in a highly condensed manner, therefore it is useful to illustrate how it is obtained. In Figure 1, we demonstrate this process in a simple example without $\text{sgn}(\Delta m_{31}^2)$ -degeneracy. We compare the often used picture in the $\delta_{\text{CP}}\text{-}\sin^2 2\theta_{13}$ -plane with the projection onto the δ_{CP} -axis, where we use exactly the same scale on the horizontal axis. In particular, we show the result in each panel with (thick curves) and without (thin curves) correlations from parameters other than $\sin^2 2\theta_{13}$.

First of all, the projection mechanism can be easily understood from this figure. If one wants to know how precisely one can measure δ_{CP} in the left panel, fixing $\sin^2 2\theta_{13}$ will inevitably lead to a too small error: The fact that we do at that time not know $\sin^2 2\theta_{13}$ more precisely than in this figure, leads to a larger error on δ_{CP} . This two-parameter correlation is well-known to affect the precision of δ_{CP} , and comes from the intrinsic structure of the oscillation probabilities. One can include it in the analysis by projection onto the δ_{CP} -axis, as it is done in the right panel. We perform this projection by minimizing (marginalizing) $\Delta\chi^2$ with respect to $\sin^2 2\theta_{13}$: If one takes the minimum $\Delta\chi^2$ in the left panel in the direction of $\sin^2 2\theta_{13}$ for each fixed value of δ_{CP} , one will find the minima along the gray curve. The projected $\Delta\chi^2$ in the right panel is then nothing else than the $\Delta\chi^2$ along the gray curve in the left panel.

Similarly to the two-parameter correlation, one can marginalize over all of the not shown parameters (within the range allowed by external data), leading to the full multi-parameter correlation. The difference between only taking into account the two-parameter correlation and the full correlation is illustrated by the difference between the thin and thick curves in both panels of Figure 1. One can easily see that, depending on the confidence level, the error can be increased by more than 100% by correlations other than with $\sin^2 2\theta_{13}$ (unlike

⁶Somewhat better results might be obtained with a T ASD (Totally Active Scintillator Detector) with about half the detector mass.

⁷Using a considerable amount of antineutrino running would also disentangle these two parameters. However, longer running times would be needed to account for the lower antineutrino cross section, which means that this scenario is unlikely to fit into the coming ten years.

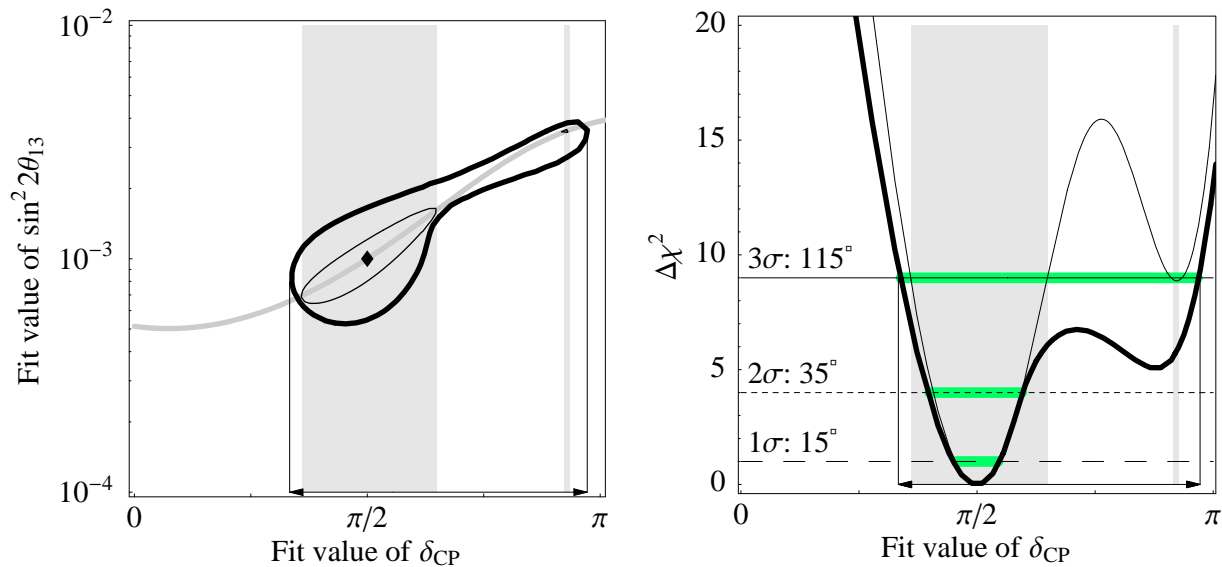


Figure 1: Correlation between δ_{CP} and $\sin^2 2\theta_{13}$ for the simulated valued $\delta_{CP} = \pi/2$ and $\sin^2 2\theta_{13} = 0.001$ for NuFact-II. The left panel shows the fit manifold in the δ_{CP} - $\sin^2 2\theta_{13}$ -plane ($\Delta\chi^2 = 9$ only), the right panel the projected $\Delta\chi^2$ onto the δ_{CP} -axis. The thin curves refer to only taking into account the correlation between δ_{CP} and $\sin^2 2\theta_{13}$, and the thick curves refer to taking into account the full multi-parameter correlation, *i.e.*, also the correlations with the parameters which are not shown. The shaded regions refer to the error in δ_{CP} for the two-parameter correlation only, whereas the arrows mark the final error including the full correlation. The left panel shows in addition in gray the curve along which the minimum $\Delta\chi^2$ in the $\sin^2 2\theta_{13}$ -direction is found. In the right panel, the finally obtained CP coverage at the 1σ , 2σ , and 3σ (1 d.o.f.) levels is marked (thick horizontal lines) and given by numbers. Standard values are used for oscillation parameters which are not shown.

being small such as often indicated in the previous literature). One can understand this mainly in terms of the $(\delta_{CP}, \theta_{13})$ -degeneracy [37], which, as a disconnected solution, may appear at a different place in the δ_{CP} - θ_{13} -plane (*cf.*, left panel, thin curve). However, if one just fixes the other (not shown) oscillation parameters, one does not account for the fact that the actual minimum may lie slightly off the shown fit manifold section (*i.e.*, plane) with respect to these parameters. The full marginalization shows the full beauty of this degeneracy.

The CP coverage in this example is obtained as the range of possible fit values which fit the simulated value $\delta_{CP} = \pi/2$. It is, for three different confidence levels, marked and given in the right panel. Note that there might be more than one fit region, which has also to be included for the CP coverage by definition. The right panel clearly shows the non-Gaussian dependence of the CP coverage on the confidence level. This dependence mainly originates in the role of the $(\delta_{CP}, \theta_{13})$ -degeneracy, which may lead to connected or disconnected degenerate solutions at the chosen confidence level. Later, we will observe that this dependency can be amplified by the $\text{sgn}(\Delta m_{31}^2)$ -degeneracy.

3.3 Localization of degeneracies

Besides the computation of the CP coverage for a specific solution in parameter space, it is necessary to find all disconnected degenerate solutions. For maximal mixing, there are up to three disconnected degenerate solutions besides the best-fit solution: one from the $(\delta_{\text{CP}}, \theta_{13})$ -degeneracy, one from the $\text{sgn}(\Delta m_{31}^2)$ -degeneracy, and one from the mixed degeneracy. Even if the $(\delta_{\text{CP}}, \theta_{13})$ -degeneracies were connected to the original solutions at the chosen confidence level, we will see later that it would in many cases be difficult to locate them only with a local minimization method.

In order to locate all degenerate solutions, we use a method based on the total event rates. To a first approximation, one can use the total neutrino and antineutrino event rates for an estimate of the positions of the degeneracies in the $\delta_{\text{CP}}\text{-sin}^2 2\theta_{13}$ -plane. These degeneracies might later be resolved by spectral information, or actually lie slightly off this plane with respect to the fixed parameters, but it turns out that this approach is rather efficient not to miss any degenerate solution. Compared to the oscillation probabilities, the total event rates already contain some energy-weighted information with respect to beam flux, cross sections, and efficiencies. This means that the position of the degeneracy can usually be more accurately determined than just using oscillation probabilities (for which one particular value of E had to be chosen, which needed to be determined by a similar algorithm).

In particular, we first compute the total rates N_0 and \bar{N}_0 of the neutrino and antineutrino appearance channels of a given experiment at the best-fit point (fixed simulated parameter values, normal mass hierarchy). Then we show the curves $N(\delta_{\text{CP}}, \sin^2 2\theta_{13})_{|\Delta m_{31}^2|>0} = N_0$ (black curve) and $\bar{N}(\delta_{\text{CP}}, \sin^2 2\theta_{13})_{|\Delta m_{31}^2|>0} = \bar{N}_0$ (gray curve) for these constant neutrino and antineutrino rates as function of δ_{CP} and $\sin^2 2\theta_{13}$, as it is illustrated in the upper left panel of Figure 2. By definition, both of these curves must go through the best-fit point marked by the star, where they intersect. It is now an interesting feature of the $(\delta_{\text{CP}}, \theta_{13})$ -degeneracy that it is indistinguishable to the best-fit solution on the total rate level [37]. Thus, the second intersection point in Figure 2 (upper left panel) directly points to the $(\delta_{\text{CP}}, \theta_{13})$ -degenerate solution. Similarly, one can flip the sign of Δm_{31}^2 and show the curves for $N(\delta_{\text{CP}}, \sin^2 2\theta_{13})_{|\Delta m_{31}^2|<0} = N_0$ and $\bar{N}(\delta_{\text{CP}}, \sin^2 2\theta_{13})_{|\Delta m_{31}^2|<0} = \bar{N}_0$, where N_0 and \bar{N}_0 are still the total rates at the best-fit point. The upper right panel of Figure 2 shows these curves for the inverted mass hierarchy, leading to two more intersections, which means that we have altogether located three (potential) degenerate solutions. Note that the shape of the curves may change, and some curves may not even intersect at all (except from the best-fit point). In the latter case, the two closest points between the curves give a hint of the position of the degeneracy.

As a next step, we start a local minimizer at each of the located degeneracies (*i.e.*, with δ_{CP} and $\sin^2 2\theta_{13}$ of each degeneracy), which minimizes the $\Delta\chi^2$ of the complete experiment simulation (including spectral information) with respect to all oscillation parameters. The resulting $(\Delta\chi^2)_{\text{min}}$ determines if a degenerate solution remains below a chosen confidence level, or if it can be immediately resolved by statistics, energy resolution *etc.*. The resulting position is the actual position of the degeneracy taking into account the complete statistical simulation. In the middle row of Figure 2, we show the results from the complete simulation, where we project the $\Delta\chi^2$ onto the $\delta_{\text{CP}}\text{-sin}^2 2\theta_{13}$ -plane. In fact, one can see that all located

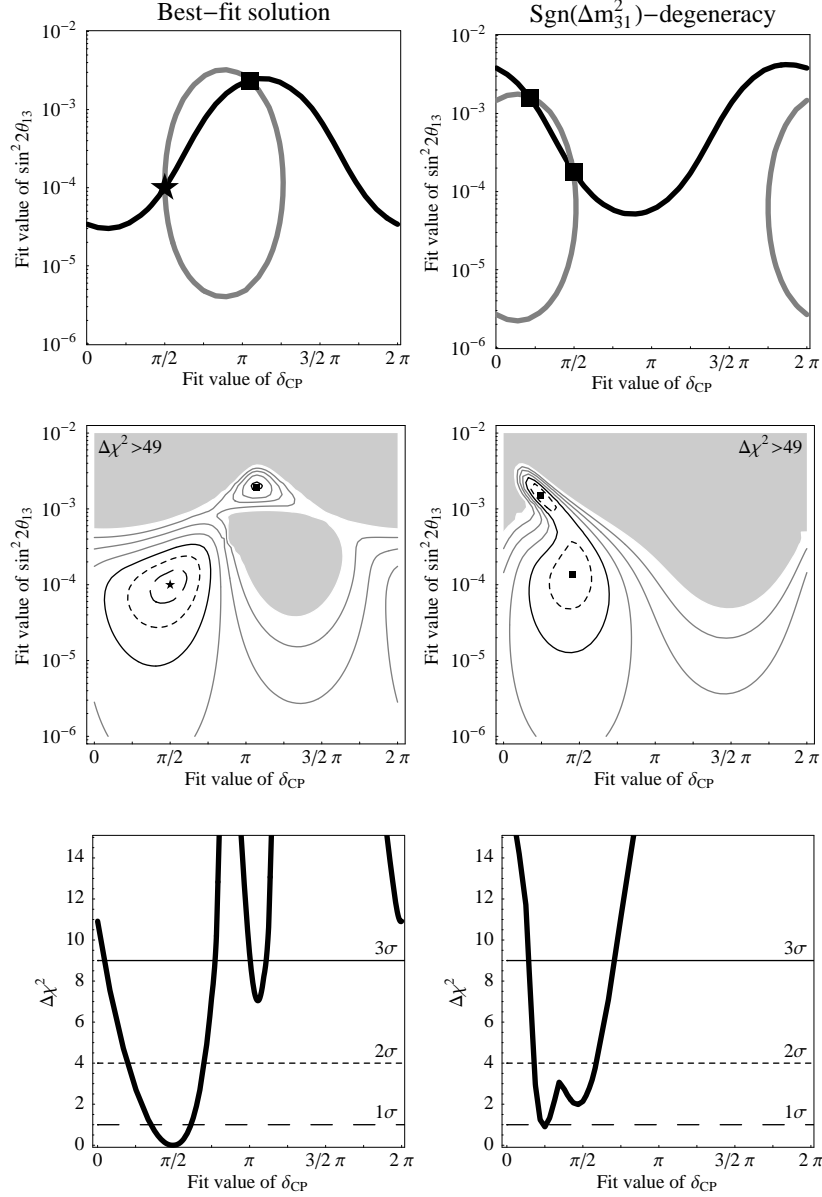


Figure 2: Degeneracy localization for the best-fit solution (left column) and $\text{sgn}(\Delta m_{31}^2)$ -degeneracy (right column) for the simulated values $\delta_{CP} = \pi/2$ and $\sin^2 2\theta_{13} = 0.0001$ and NuFact-II. The first row shows the total neutrino (black) and antineutrino (gray) constant rate curves as described in the text. The second row shows the projections of the fit manifolds onto the δ_{CP} - $\sin^2 2\theta_{13}$ -plane, where the 1σ (long dashed), 2σ (short dashed), 3σ (solid black), 4σ , 5σ , and 6σ (gray curves) contours (1 d.o.f.) are shown. The gray-shaded region corresponds to $\Delta\chi^2 > 49$. The third row shows the projection of the second row onto the δ_{CP} -axis, from which the final CP coverage is read off. In some of the panels, stars refer to the best-fit solution, and filled rectangles to the located degeneracies. Standard values are used for oscillation parameters which are not shown.

degeneracies are in this case present below the 3σ confidence level, and that their positions are very close to the initial guesses from the total rate method.

Eventually, we show in the lower row of Figure 2 the final $\Delta\chi^2$ which is projected onto the δ_{CP} -axis. Note that for a given set of simulated parameters, the final CP coverage is obtained as union of all CP-ranges fitting the simulated value. Therefore, one should think about an overlay between the left and right panels to find the ranges which fit the simulated value of δ_{CP} . From the comparison between the middle and lower rows of Figure 2, we can demonstrate some more interesting properties of the topology for small values of $\sin^2 2\theta_{13}$, too. First of all, as it can be inferred from the left panels, in order to project onto the δ_{CP} -axis, it is not sufficient to start the local minimizer at the best-fit value of $\sin^2 2\theta_{13}$. In this specific case, one can easily image that starting the minimizer at $(\pi, 10^{-4})$ could make it run back towards smaller values of $\sin^2 2\theta_{13}$ instead of larger ones, where the degeneracy is actually located. Therefore, the information from the total rate approach is very useful to obtain an initial “guess” of the value of $\sin^2 2\theta_{13}$ where the degeneracy is located at. Another interesting feature appears in the projected $\Delta\chi^2$ in the lower right panel. In this figure, the $\Delta\chi^2$ is actually not a differentiable function, which seems to be very artificial at the first sight. However, the comparison with the middle right panel clearly illustrates the jump in $\sin^2 2\theta_{13}$ when moving from the left to the right in δ_{CP} . Again, only using some of the information from the first row would not reveal the true structure of this topological feature.

In summary, this total-rate-based approach turns out to be very powerful for the localization of degeneracies and dealing with the topology of neutrino factories for small values of $\sin^2 2\theta_{13}$. In principle, it can be also applied to the eight-fold degeneracy, where the operation $\theta_{23} \rightarrow \pi/2 - \theta_{23}$ leads to four more possible solutions.

3.4 Effects and interpretation of degeneracies

In order to understand the effects of the degeneracies better, we show an illustrative example in Figure 3. In this figure, the projected $\Delta\chi^2$ is shown for the simulated value $\delta_{\text{CP}} = 0$ and several increasing simulated values of $\sin^2 2\theta_{13}$ as given in the plot captions. Both the original solutions (black curves) and the $\text{sgn}(\Delta m_{31}^2)$ -degeneracies (gray curves) are plotted. For the smallest value of $\sin^2 2\theta_{13}$ (first panel), there is no sensitivity to δ_{CP} at the 2σ and 3σ confidence levels. The $\Delta\chi^2$ is flat in a wide region, where $\sin^2 2\theta_{13} = 0$ acts as an attractor to the minimizer. At the 1σ confidence level, however, the degeneracy appears at a different position in δ_{CP} , which can easily double the CP coverage. Thus, we learn that the degeneracy becomes especially important if it introduces new values of δ_{CP} compared to the original solution. Note again that the final CP coverage is obtained as the union of all regions fitting the true value, because any value within a degenerate solution cannot be excluded at the chosen confidence level.

For somewhat larger values of $\sin^2 2\theta_{13}$ (second panel), the minimum of the degeneracy is lifted. In this example, there is also a $(\delta_{\text{CP}}, \sin^2 2\theta_{13})$ -ambiguity in both the original and $\text{sgn}(\Delta m_{31}^2)$ -degenerate solution, but only the one of the $\text{sgn}(\Delta m_{31}^2)$ -degeneracy affects the results below the 3σ confidence level. In particular, it approximately doubles the size of the 2σ -allowed region. In this case, the original and degenerate solutions hardly overlap,

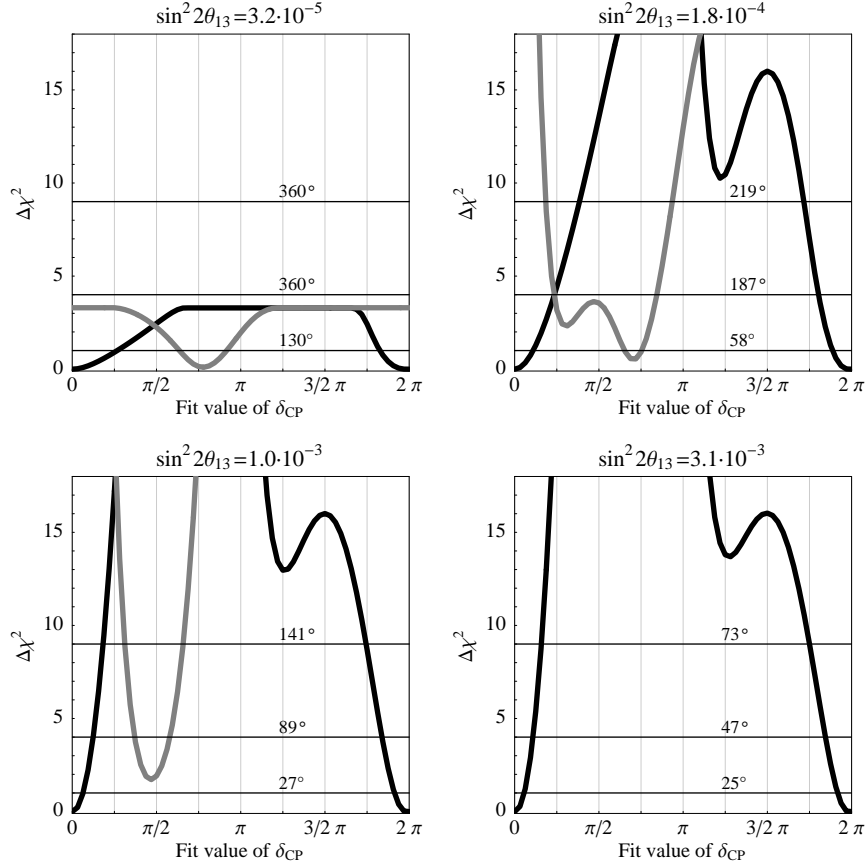


Figure 3: The projected $\Delta\chi^2$ for the simulated value $\delta_{\text{CP}} = 0$ and several (increasing) simulated values of $\sin^2 2\theta_{13}$ as given in the plot captions (NuFact-II). In each figure, the original solution (black curve) and the $\text{sgn}(\Delta m_{31}^2)$ -degeneracy (gray curve) is shown (degeneracy only shown if appearance below 3σ confidence level). In addition, the final values of the CP coverage are given. For the other oscillation parameters, we use the standard values for this study.

and the CP coverage of the original solution is almost tripled at the 2σ confidence level. Because of the increasing overlap at larger $\Delta\chi^2$ -values, it does not change very much at the 3σ confidence level, which is another indicator for a strongly non-Gaussian behavior of the CP coverage.

For even larger values of $\sin^2 2\theta_{13}$ (right two panels), the $\text{sgn}(\Delta m_{31}^2)$ -degeneracy is lifted until it does not appear below the 3σ confidence level anymore. The $(\delta_{\text{CP}}, \sin^2 2\theta_{13})$ -ambiguity in the $\text{sgn}(\Delta m_{31}^2)$ -degeneracy (mixed degeneracy) can be resolved by the better statistics in the appearance channels. Reading Figure 3 as a movie from left to right (not to scale), it is obvious that problems with degeneracies especially occur at an intermediate scale $10^{-4} \lesssim \sin^2 2\theta_{13} \lesssim 5 \cdot 10^{-3}$, where the fit topology is rather flat. Another important aspect in the effects of degeneracies is not so obvious from this figure: For simulated values in the region of $\delta_{\text{CP}} \sim 3/2 \cdot \pi$ the degeneracy starts moving with increasing $\sin^2 2\theta_{13}$. This has been illustrated in Figure 8 of Ref. [45], where especially the position of the degeneracy

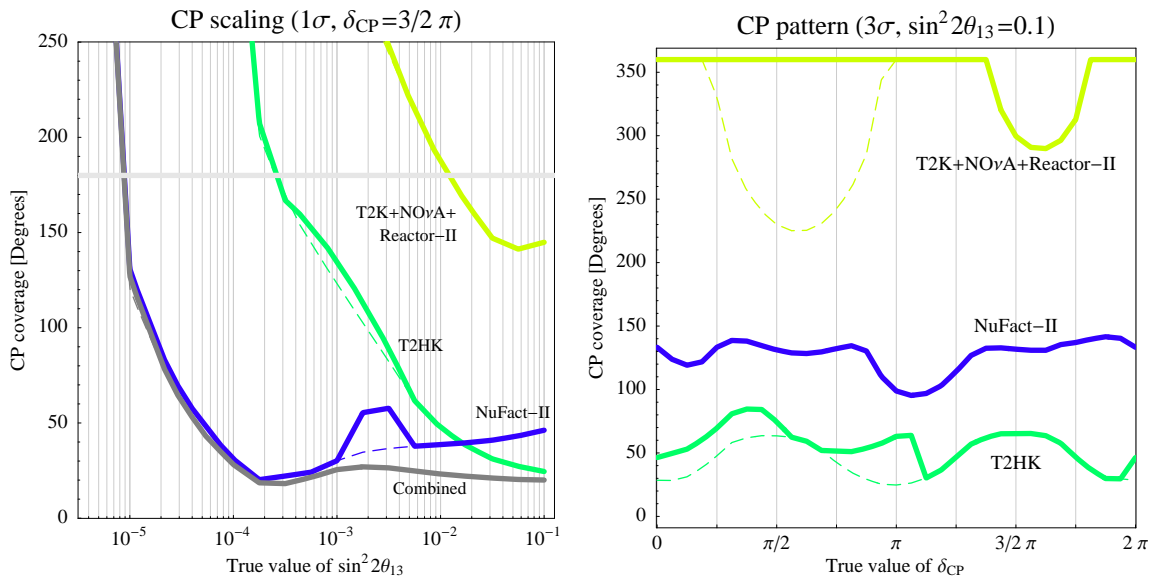


Figure 4: The CP coverage as function of the true value of $\sin^2 2\theta_{13}$ (“CP scaling”) and as function of the true value of δ_{CP} (“CP pattern”) for different experiments and parameters as given in the figures. The thin dashed curves refer to not taking into account the $\text{sgn}(\Delta m_{31}^2)$ -degeneracy, *i.e.*, if the mass hierarchy was known. The horizontal line (left panel) is an estimate for the range of values (below line), where CP violation measurements become possible. Standard values are used for the oscillation parameters which are not shown. Note that the two figures use different confidence levels and different scales in the CP coverage.

close to π (“ π transit”) destroys the CP violation sensitivity ($\sin^2 2\theta_{13} \sim 3 \cdot 10^{-4}$). Thus, the structure of the topology strongly depends on the simulated parameter values, which lead to a certain, in some cases complex configuration and shape of original and degenerate solutions. Therefore, we cannot expect to understand every feature of the CP coverage without analyzing the respective topology.

4 From exclusion to high precision measurements of δ_{CP}

In this section, we focus on the comparison of different classes of experiments, and we demonstrate the conceptual differences arising when going from one to the next generation of experiments. It is not sufficient to show only the CP coverage for some discrete sets of parameter values in order to gain further insights. We therefore define highly condensed performance indicators (HCPI) as function of the most relevant parameter values. For the case of CP coverage it turns out that the dependence on the true (simulated) value of $\sin^2 2\theta_{13}$, and the true value of δ_{CP} itself are the most interesting parameter dependencies. Though the latter seems to be strange at a first glance, it is exactly what was seen in Section 2, namely that the topology depends on the value of δ_{CP} actually realized by nature. Thus, the correct way to interpret these functional dependencies is to read: “If the true value of the parameter ... is ..., the CP coverage will be ... degrees.”.

In particular, we use the following two HCPI:

CP scaling: This is the CP coverage as function of the true value of $\sin^2 2\theta_{13}$ (for fixed simulated value of δ_{CP}). It is useful to compare the performance of different experiments as function of $\sin^2 2\theta_{13}$ and it is mainly constrained by the statistics of the appearance channels.

CP pattern: Defined as CP coverage as function of the true value of δ_{CP} (for fixed simulated value of $\sin^2 2\theta_{13}$) [61]. It is useful for a minimization of the risk with respect to the unknown true value of δ_{CP} and it is mainly determined by the intrinsic structure of the oscillation probability in Eq. (1).

Examples for a CP scaling and a CP pattern can be found in Figure 4. With the GLoBES software [79], each of these figures takes several days of computation time on a modern computer, because about 10^9 $\Delta\chi^2$'s have to be evaluated.

An even more condensed performance indicator for CP scalings can be found in Figure 19 of Ref. [45], which takes the conservative case over all simulated values of δ_{CP} (instead of fixing δ_{CP}). One can easily imagine that, with reasonably good resolution, such a figure has even an order of magnitude longer computation time including all correlations and degeneracies than the ones shown in this study.

4.1 Comparison of experiment classes

In Figure 4, left panel, we compare different classes of experiments, where the figure is shown at the 1σ confidence level for fixed true $\delta_{\text{CP}} = 3\pi/2$. One class of these experiments is the combined potential of the next generation of experiments under optimistic assumptions. For the combination T2K+NO ν A+Reactor-II, where the large reactor experiment could equally be replaced by extensive antineutrino running, already some exclusion of the parameter space of δ_{CP} might be possible. In particular, for the shown parameter values, up to about 210° ($360^\circ - 150^\circ$) of all possible values could be disfavored at the 1σ confidence level, where next generation experiments are limited to the range $\sin^2 2\theta_{13} \gtrsim 10^{-3}$. Note that a CP precision smaller than 180° is a necessary condition for maximal CP violation measurements, which means that CP violation measurement with the shown combination will be hardly possible at a useful confidence level (*cf.*, horizontal line in left panel). In addition, as one can see from Figure 4, right panel, a CP coverage smaller than 360° is only available close to $3\pi/2$ (for which the left panel is shown).

As a representative for superbeam upgrades, we have shown T2HK in both panels. Since we assume a fiducial mass of 1 Mt, it represents the upper possible limit for superbeams. As one can see from Figure 4, left panel, T2HK could give precise information on δ_{CP} in the range $\sin^2 2\theta_{13} \gtrsim 10^{-3}$: In about this range, (maximal) CP violation measurements are possible (*cf.*, Figure 18 of Ref. [45]). In addition, for $\sin^2 2\theta_{13} \gtrsim 10^{-2}$ the information would be better than the one from the neutrino factory. The right panel of Figure 4 clearly demonstrates that for large values of $\sin^2 2\theta_{13}$ very good CP precision measurements are possible regardless the true value of δ_{CP} . In particular, it has been demonstrated in Refs. [45, 59] that for large

values of $\sin^2 2\theta_{13}$ neutrino factories can be highly affected by matter density uncertainties, which means that the superbeam upgrade could actually be more competitive.

On the end of very small values of $\sin^2 2\theta_{13}$, neutrino factories could give information on δ_{CP} down to $\sin^2 2\theta_{13} \sim 10^{-5}$ (*cf.*, Figure 4, left panel). Especially in combination with T2HK, the CP coverage becomes very flat in $10^{-4} \lesssim \sin^2 2\theta_{13} \lesssim 10^{-1}$. As far as the dependence on the true value of δ_{CP} is concerned (right panel), the dependence is rather flat for large values of $\sin^2 2\theta_{13}$ because of the relatively broad energy spectrum. However, we will see later, that this behavior changes for smaller values of $\sin^2 2\theta_{13}$. Thus, in some sense, the parameter values for the two panels in Figure 4 are chosen that both figures look very smooth and show all investigated experiments. Nevertheless, Figure 4 shows the quite generally applicable rule that the true value of $\sin^2 2\theta_{13}$ determines the class of reasonable experiments [84]. This can be understood in terms of the statistics in the appearance channel in Eq. (1): The “signal” in the second and third terms is simply proportional to $\sin 2\theta_{13}$, which means that the more events one has in this channel, the smaller values of $\sin^2 2\theta_{13}$ allow the extraction of δ_{CP} . Thus, there is no surprising result in the CP scalings. The CP patterns, however, will need further illumination in the next subsections.

4.2 Characteristics of superbeams and the role of reactor experiments

Superbeams have some common characteristics, no matter if next-generation experiments, or high-end superbeam upgrades. In particular for the ones discussed here using the off-axis technology [85], the beam spectrum becomes very narrow. The $(\delta_{\text{CP}}, \theta_{13})$ -degeneracy does usually not appear in the topology and causes no major problems. Neglecting the $\text{sgn}(\Delta m_{31}^2)$ -degeneracy, the dependence of the CP coverage on the confidence level is therefore rather Gaussian. In the analysis, there are hence no major complications expect from the $\text{sgn}(\Delta m_{31}^2)$ -degeneracy.

For these “quasi-monochromatic” beams, there is only little spectral information, which means that many of their properties can be understood on the oscillation probability or total rate level. One such interesting approach are bi-probability or bi-rate graphs [61, 72, 86], which are explicitly targeted towards understanding CP phase-dependent properties. In particular, CP patterns for superbeams, such as in Figure 4, right panel, can be understood in terms of bi-rate graphs [61], where different regimes can be distinguished: For very high statistics, one obtains the typical dependence as one would expect from the $\sin \delta_{\text{CP}}$ -term discussed in Section 2 (for example, Figure 4, right panel, for T2HK, dashed curve). For very poor statistics or large systematical errors, the dependence on δ_{CP} is reverted (*cf.*, Figure 4 of Ref. [61], left panel). For intermediate statistics, this behavior can, in particular in connection with the $\text{sgn}(\Delta m_{31}^2)$ -degeneracy, lead to very complicated CP patterns (*cf.*, Figure 4 of Ref. [61], middle panel). In addition, the $\text{sgn}(\Delta m_{31}^2)$ -degeneracy affects superbeam measurements especially in the first and second quadrants, which means that superbeam measurements are usually best between π and 2π [61, 72]. To summarize, the dependence on δ_{CP} can be understood, though it might be complicated. For T2HK, the strongest amplitude can be found for $\sin^2 2\theta_{13} \lesssim 10^{-3}$, which can vary between 150° and 360° by more than a factor of two – between CP violation measurements possible and no information on δ_{CP} at all [61].

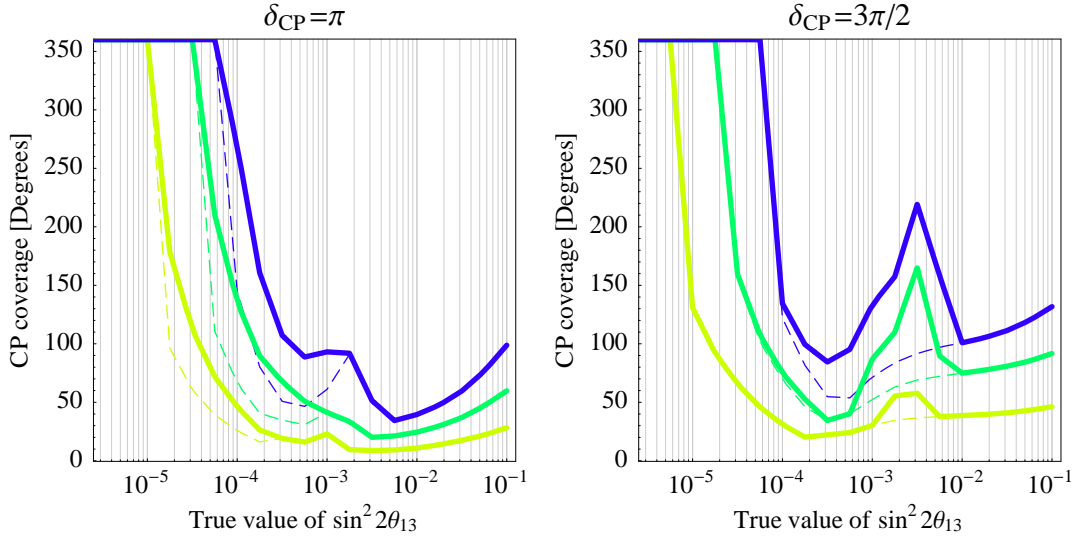


Figure 5: CP scalings for NuFact-II and two different selected values of $\sin^2 2\theta_{13}$ as given in the plot captions. The different curves in different colors correspond to the 1σ , 2σ , and 3σ confidence levels (from the lowest to the highest), where the dashed curves correspond to not taking into account the $\text{sgn}(\Delta m_{31}^2)$ -degeneracy. For the not shown oscillation parameters, we use the standard values for this study.

Future reactor experiments could for $\sin^2 2\theta_{13} \gtrsim 10^{-2}$ help to resolve the correlation between $\sin^2 2\theta_{13}$ and δ_{CP} by a precision measurement of $\sin^2 2\theta_{13}$ instead of extensive antineutrino running at superbeams [2, 82, 87]. As it has been demonstrated in Ref. [61] (*cf.*, Figure 3), there are no major qualitative differences for the CP patterns using antineutrino running or a large reactor experiment. Therefore, the contribution of reactor experiments to CP measurements can be understood in a similar way as the antineutrino running mode at a superbeam.

4.3 Characteristics of neutrino factories

As we have illustrated in Section 3, the analysis of neutrino factories is much more complicated than the one for superbeams because of the complicated topology. In particular, we can not only expect a strong dependence on $\sin^2 2\theta_{13}$ or δ_{CP} itself, but also on the confidence level because of lifted (in CL) or moving (in δ_{CP}) degeneracies and the importance of the relative position to the best-fit solution. In addition, neutrino factories carry very good spectral information, which means that a simple interpretation in terms of bi-rate graphs is not possible. However, we will demonstrate how one can understand certain features and limiting cases.

Let us first of all discuss the CP scaling for two selected, very different cases in Figure 5. Obviously, the shape of these scalings strongly depends on the confidence level and the true value of δ_{CP} . In particular, we need to distinguish irregularities in the dashed curves (no $\text{sgn}(\Delta m_{31}^2)$ -degeneracy), which are caused by the $(\delta_{\text{CP}}, \theta_{13})$ -degeneracy, and irregularities which are only present in the thick curves, which are caused by the $\text{sgn}(\Delta m_{31}^2)$ - or mixed

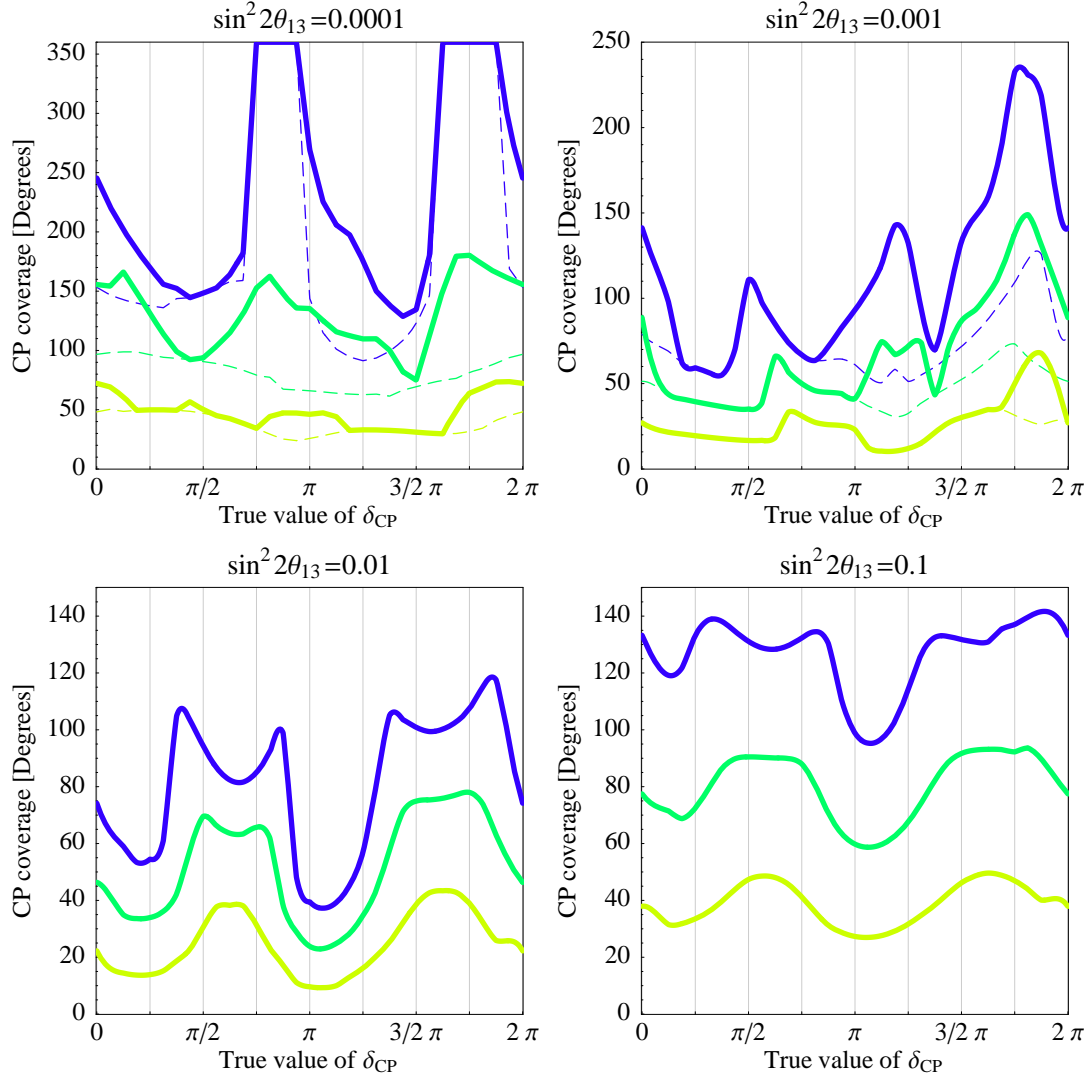


Figure 6: CP patterns for NuFact-II and different values of $\sin^2 2\theta_{13}$ as given in the plot captions. The different curves in different colors correspond to the 1σ , 2σ , and 3σ confidence levels (from the lowest to the highest), where the dashed curves correspond to not taking into account the $\text{sgn}(\Delta m_{31}^2)$ -degeneracy. For the not shown oscillation parameters, we use the standard values for this study.

degeneracies. If we only concentrate on the 3σ curves (dark curves), we find that there are major irregularities caused by the $\text{sgn}(\Delta m_{31}^2)$ - or mixed degeneracies in both cases. However, for $\delta_{\text{CP}} = \pi$ (left panel), also the thick curve is not smooth, which is due to the $(\delta_{\text{CP}}, \theta_{13})$ -degeneracy being present around $\sin^2 2\theta_{13} \lesssim 10^{-3}$. For the case $\delta_{\text{CP}} = 3\pi/2$ (right panel), the mixed degeneracy (*i.e.*, the $(\delta_{\text{CP}}, \theta_{13})$ -ambiguity in the $\text{sgn}(\Delta m_{31}^2)$ -degeneracy) doubles the CP coverage close to $2.5 \cdot 10^{-3}$. In general, degeneracies affect mainly the higher confidence levels, since they usually disappear below a specific value of $\Delta\chi^2$. In addition, note that these interpretations cannot be solely made from Figure 5, which means that one

has to look at less condensed information.

The CP patterns for NuFact-II are shown in Figure 6 for different values of $\sin^2 2\theta_{13}$. As we have indicated above, their interpretation is much more complicated than for superbeams because of spectral information. First of all, note that there can be up to a factor of five difference between the smallest and largest values of the CP coverage, such as for $\sin^2 2\theta_{13} = 0.001$ (3σ CL). This alone is a major hint that one should always compare the complete CP patterns of different experiments and not only the results for different selected values of δ_{CP} ⁸. Compared to superbeams, we find similar principle cases:

High-statistics-dominated region (large $\sin^2 2\theta_{13}$): The best performance can be achieved where the $\sin \delta_{\text{CP}}$ -term in Eq. (1) has the steepest slope, *i.e.*, close to 0 and π . This can be clearly seen for $\sin^2 2\theta_{13} = 0.1$, 1σ CL. For larger confidence levels, however, the broad spectrum makes the dependence on δ_{CP} flatter.

Degeneracy-dominated region At intermediate values of $\sin^2 2\theta_{13} \simeq 10^{-3}$ the four terms in Eq. (1) have all approximately the same size, hence the problem of disentangling them is worst for those values of $\sin^2 2\theta_{13}$. Thus the relative position and appearance of the degeneracies is the major impact factor describing the CP pattern and can lead to complicated structures.

Low-statistics-dominated region (small $\sin^2 2\theta_{13}$): The behavior is inverted (best performance close to $\pi/2$ and $3\pi/2$) because of the relatively large statistical errors, which can be understood in terms of bi-rate graphs (compare 3σ curve for $\sin^2 2\theta_{13} = 0.0001$ in Figure 6 to the corresponding Figure 4 for T2HK of Ref. [61], left panel). The spectral information is in this case a subleading effect.

Especially, the second case of the degeneracy-dominated regime is very interesting. Analyzing the 3σ curve of Figure 6 for $\sin^2 2\theta_{13} = 0.001$ (with the help of less condensed information), the different peaks can be explained as follows: The first peak close to $\delta_{\text{CP}} = \pi/2$ is an effect of the $(\delta_{\text{CP}}, \theta_{13})$ -degeneracy present for values of δ_{CP} in this range. The peak close to $5\pi/4$ comes from the $\text{sgn}(\Delta m_{31}^2)$ -degeneracy. This degeneracy, however, moves as function of δ_{CP} and overlaps the best-fit region for $11\pi/8$ almost exactly, which leads to the sharp minimum. For larger values of δ_{CP} , not only the $\text{sgn}(\Delta m_{31}^2)$ -degeneracy becomes effective again (because it moves away from the original solution), but also the $(\delta_{\text{CP}}, \theta_{13})$ -degeneracy in the original solution and the same in the $\text{sgn}(\Delta m_{31}^2)$ -degeneracy (mixed degeneracy). Close to $7\pi/4$ the overall four-fold degeneracy is present with maximum non-overlap in δ_{CP} -space, leading to the extremely high peak. One important consequence of the moving degeneracy close to $\delta_{\text{CP}} = 3\pi/2$ (*cf.*, Figure 8 of Ref. [45]) is that the neutrino factory is highly affected by degeneracies in the third and fourth quadrants. This behavior is very complementary to the one of the superbeams, which are mainly affected in the first and second quadrants. This explains the synergy between superbeams and neutrino factories in certain regions of the parameter space [43].

⁸In other words: One can more or less always choose δ_{CP} in such a way that some experiment is better than the other one.

5 Synergies in future high-precision measurements

Eq. (1) shows that the actual value of $\sin^2 2\theta_{13}$ is the missing key parameter for any measurement of δ_{CP} . We will therefore organize the discussion of synergies for precision measurements of δ_{CP} by the true value of $\sin^2 2\theta_{13}$, *i.e.*, the value which is actually extracted from experiments (and corresponds to the simulated value for simulations). Then we will discuss relevant synergies for high precision measurements of δ_{CP} using a more conceptual line of reasoning.

5.1 The impact of the true $\sin^2 2\theta_{13}$

Unless a finite value of $\sin^2 2\theta_{13}$ is measured, each generation of experiments will push the upper bound towards smaller values. One might argue therefore, that a finite value of $\sin^2 2\theta_{13}$ has to be established before it makes sense to discuss a measurement of δ_{CP} . However, in fact these two parameters will in most cases (except from reactor experiments) be simultaneously accessible, *i.e.*, a positive signal for $\sin^2 2\theta_{13}$ comes together with some information on δ_{CP} . Taking Figure 4, left panel, as a rough estimate for the sensitivity to δ_{CP} , we find the following approximate regions in $\sin^2 2\theta_{13}$:

$\sin^2 2\theta_{13} \gtrsim 10^{-2}$: In this case, $\sin^2 2\theta_{13} > 0$ will be very likely established by a superbeam or reactor experiment. The measurement of δ_{CP} could then be pushed by existing superbeam experiments or upgraded versions (new baselines, new or larger detectors, more protons, longer running times, different L/E 's *etc.*). The discussion of synergies then reduces to the level of superbeams and reactor experiments [46, 50, 57, 82, 86–89]. However, as one can also read off Figure 4 (left panel), for a high precision measurement of δ_{CP} , a very large superbeam upgrade, such as T2HK, is the choice to go for. Already one such experiment, which encapsulates the synergy between the neutrino and antineutrino running, could deliver excellent information on δ_{CP} . On the other hand, from the point of δ_{CP} , a neutrino factory is not needed to obtain high precision results (maximal mixing assumed). In particular, as it is illustrated in Figure 6 of Ref. [59], matter density uncertainties highly affect the CP precision measurement for large values of $\sin^2 2\theta_{13}$. Effectively, they act as a normalization uncertainty of the first term in Eq. (1), which makes it hard to extract the second and third ones.

$10^{-3} \lesssim \sin^2 2\theta_{13} \lesssim 10^{-2}$: This is one of the most interesting ranges for this synergy discussion, because it goes beyond the reach of next generation experiments, but it is well within the reach of superbeam upgrades and other alternative technologies (such as silver channel measurements or β -Beams) [9, 42–44, 51, 90–93].

$10^{-4} \lesssim \sin^2 2\theta_{13} \lesssim 10^{-3}$: In this region, neutrino factories are the top candidates, which, however are highly affected by degeneracies. This essentially means that the discussion of synergies reduces to the one of two neutrino factory baselines, such as in Refs. [37, 55]. In particular, it has been demonstrated in Ref. [55] that the combination 3000 km + 7500 km (“magic baseline”, *cf.* Section 2) is the optimal choice for $\sin^2 2\theta_{13}$ (and other measurements). We will therefore test this configuration for precision

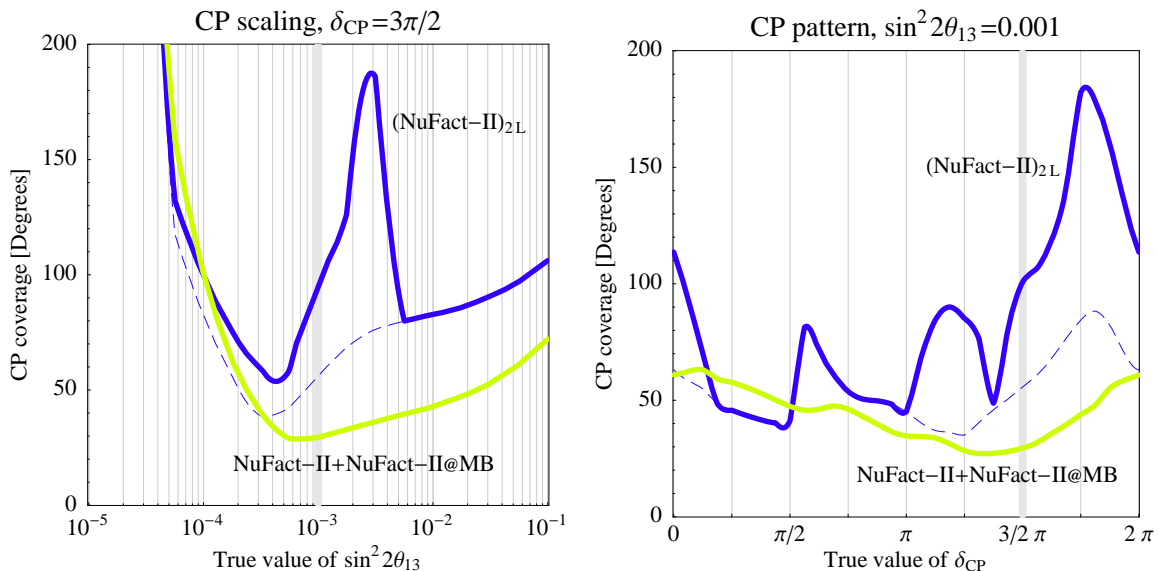


Figure 7: The CP scaling and CP pattern for NuFact-II and the oscillation parameters given in the figure captions (3σ confidence level). The dark curves correspond to NuFact-II at $L = 3000$ km, but with double luminosity (2L). The light curves corresponds to NuFact-II with two detectors, which are located at $L = 3000$ km and $L = 7500$ km (“magic baseline” = MB) and operated with single luminosities each. This means that the product of useful muon decays times overall detector mass is equal in both shown cases. The dashed curves refer to not taking into account the $\text{sgn}(\Delta m_{31}^2)$ -degeneracy. The vertical lines mark the parameter values for which the plots correspond to each other. Standard values are used for the oscillation parameters which are not shown.

measurements of δ_{CP} . So far, the only other competitive technology for $\sin^2 2\theta_{13} \lesssim 10^{-3}$ could be high-gamma β -Beams [9], but their physics potential has to be evaluated further [83]. Note that the combination, for instance, with a superbeam would not help much below $\sin^2 2\theta_{13} \lesssim 10^{-3}$, as it can be seen from Figure 4, left panel.

$10^{-5} \lesssim \sin^2 2\theta_{13} \lesssim 10^{-4}$: Only neutrino factories (and maybe high-gamma β -beams) could access this range. As we will see later, we are now for CP precision measurements in the (poor) statistics dominated regime, which means that correlations and degeneracies become a secondary impact factor. The discussion of synergies is the obsolete and reduces to an optimization of the statistics. One neutrino factory baseline would probably be sufficient in this case.

$\sin^2 2\theta_{13} \lesssim 10^{-5}$: This case needs further study. However, if one really wants to built an experiment if $\sin^2 2\theta_{13}$ has not been found at a neutrino factory, it is likely that a substantial luminosity increase will be needed.

5.2 One versus two neutrino factory baselines

Since a neutrino factory muon storage ring has (at least) two straight sections, the option of a second detector should be natural when planning the storage ring geometry. As it has been discussed in Section 2, the “magic baseline” of about 7 500 km has turned out to be optimal for a “clean” measurement of $\sin^2 2\theta_{13}$ [55] and very good for CP violation measurements [37]. This means that one could suspect very good synergy effects for high precision measurements of δ_{CP} , since the correlation and degeneracy between δ_{CP} and θ_{13} could be easily disentangled. As discussed in Section 5.1, the relevant parameter space region for this option is $10^{-4} \lesssim \sin^2 2\theta_{13} \lesssim 10^{-2}$.

In Ref. [46], “synergy” between two or more experiments/options has been defined as the “extra gain [...] beyond the simple addition of statistics”. Thus, in order to compare the potential of one and two neutrino factory baselines, it is not enough to simply add another baseline and compare it to the single baseline option, *i.e.*, one has to “subtract” the effect of the extra statistics. We therefore compare in Figure 7 the potential of a one- and two-baseline neutrino factory by using the double luminosity for the single baseline option, which means that both options are using the same product of useful muon decays times overall detector mass. Thus, given a total amount of detector mass, it refers to the question if one should put it all to 3 000 km, or a part of it (in our case half) to 7 500 km. As performance indicators, we choose the CP scaling for $\delta_{\text{CP}} = 3\pi/2$ and the CP pattern for $\sin^2 2\theta_{13}$, since we know from the discussion in Section 4 that these choices of parameters represent the most critical regions within the parameter space. In particular, it can be read off the right panel of Figure 7 that $\delta_{\text{CP}} = 3\pi/2$ is well within a region where degeneracies are present, and it can be read off the left panel of Figure 7 that $\sin^2 2\theta_{13} = 0.001$ is in the critical range. Besides that, $\sin^2 2\theta_{13} = 0.001$ is in the middle of the parameter range of interest here.

The CP scaling in Figure 7, left panel, is an important indicator to discuss the synergy between two neutrino factory baselines in the complete parameter range of interest in $\sin^2 2\theta_{13}$. It turns out that in the complete range $10^{-4} \lesssim \sin^2 2\theta_{13} \lesssim 10^{-2}$ there is a real synergy between the 3 000 km baseline and the magic baseline. In particular, the effect can be up to half of the parameter space for δ_{CP} . One can also see from this panel that below $\sin^2 2\theta_{13} \lesssim 10^{-4}$ the 3 000 km baseline alone is actually doing better, which is the low-statistics-dominated region discussed in Section 5.1.

The CP pattern in Figure 7, right panel, is the risk assessment indicator with respect to the unknown true value of δ_{CP} . As one can see from the curve for $(\text{NuFact-II})_{2\text{L}}$, there is a range for the CP coverage from 40° to 190° , *i.e.*, almost a factor of five. Not only can the minimum of this range be reduced with the magic baseline option, *i.e.*, the performance at the best point, but also the amplitude to about 40° compared to 150° before. Thus, the risk of ending up with a very poor measurement of δ_{CP} – just because nature was not kind – is substantially lowered. However, it is important to note that there are regions in parameter space where no synergy is needed because problems with correlations and degeneracies are small. In particular, the single baseline option does very well in the first quadrant, which means that the second baseline would be a waste of resources in this case. Thus, we conclude that one should definitively design the muon storage ring for these two baselines. However,

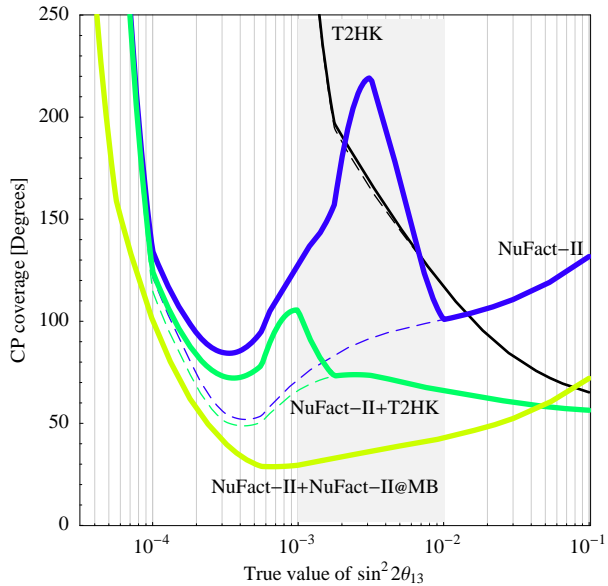


Figure 8: The CP scaling for the experiments as given in the figure (3σ confidence level, $\delta_{\text{CP}} = 3\pi/2$). The dashed curves refer to not taking into account the $\text{sgn}(\Delta m_{31}^2)$ -degeneracy. The shaded region corresponds to the $\sin^2 2\theta_{13}$ -range where synergy effects with the superbeam are present. For the other oscillation parameters, we choose the standard values from this study. Details about the setups indicated by the labels can be found in the text.

one may use a staged approach with adding the second detector later.⁹

5.3 Superbeam upgrade plus neutrino factory?

As it has been pointed out in Section 4, superbeams and neutrino factories have a complementary behavior in δ_{CP} -space if δ_{CP} is in the third or fourth quadrants. Therefore, it is a natural question to ask for the synergy between superbeam upgrades and neutrino factories [43]. In this case, it is not obvious how to show synergy effects, *i.e.*, how to distinguish between addition of statistics and real gain in physics potential. In order to test this synergy, we show in Figure 8 the CP scalings for NuFact-II, T2HK, NuFact-II+T2HK, and NuFact-II+Nufact-II@MB ($L = 3000$ km plus $L = 7500$ km at “Magic Baseline”) for $\delta_{\text{CP}} = 3\pi/2$. First of all, one can see from this figure that the combination of NuFact-II and T2HK indeed performs much better than the individual experiments. In fact, in comparison with $(\text{NuFact-II})_{2L}$, one can show that there is a real synergy effect in $10^{-3} \lesssim \sin^2 2\theta_{13} \lesssim 10^{-2}$. However, there is no real gain below $\sin^2 2\theta_{13} \lesssim 10^{-3}$ except from adding a bit of statistics, which confirms that superbeam upgrades would not help much below $\sin^2 2\theta_{13} \lesssim 10^{-3}$. As far as the CP pattern is concerned, one can show that the synergy effect is restricted to the third and fourth quadrants, which means that the combination with a superbeam upgrade

⁹Note that the muon storage ring tunnel for the 7500 km option might actually be a major cost factor compared to the second detector because of the strong decay tunnel slope. As well as the installation of the beam pipe and magnets at such a steep angle. Therefore, the staged approach might be a good solution.

only helps in a part of the parameter space.

One can now ask the question if one should have a superbeam upgrade or a second neutrino factory baseline instead. If we assume that the neutrino factory is necessary for the gray-shaded range in Figure 8, *i.e.*, that it will be built anyway, it could be fair to compare the additional effort for the magic baseline (including 50 kt detector) with the megaton water Cherenkov detector necessary for T2HK. Comparing the respective curves in Figure 8, the magic baseline option is about a factor of two better in the discussed $\sin^2 2\theta_{13}$ -range. Since there is no real synergy effect between neutrino factory and superbeam upgrade below $\sin^2 2\theta_{13} \lesssim 10^{-3}$ anymore, this ratio increased to about a factor of three there. Thus, if $\sin^2 2\theta_{13}$ turns out to be smaller than 10^{-3} , the superbeam upgrade would not help.

5.4 Other cases: Alternative technologies or non-maximal mixing

The last three subsections have focused on reasonably well-established technologies and the current best-fit case of maximal atmospheric mixing. In this subsection, we will qualitatively discuss possible alternatives to these scenarios.

Except from different detector technologies, the most interesting alternative beam could be a β -beam [8, 94]. In particular, if a higher gamma β -beam [9] is feasible, then it could be a real competitor to neutrino factories. Another challenging conceptual alternative for synergy effects is the ν_τ appearance “silver” channel [44, 51]. We do not analyze these options quantitatively in this study, since it is premature to anticipate the most promising direction on the relevant time scales. In addition, there are different technological questions to be clarified, and the analysis would therefore go far beyond the scope of this work. However, for the precision of δ_{CP} , we can qualitatively formulate the requirements of a competitor to a neutrino factory from Figure 7 (including maximal potential, *i.e.*, “magic baseline” option):

The *alternative* configuration should be able to measure δ_{CP} in the *full range* $10^{-4} \lesssim \sin^2 2\theta_{13} \lesssim 10^{-2}$ and $0 \lesssim \delta_{\text{CP}} < 2\pi$ to about 50° at the 3σ confidence level (including all correlations and degeneracies).

Similarly, if we assume that we have a neutrino factory with one baseline, the requirement for synergy effects reads

The *complementary* experiment should be able to provide good information on δ_{CP} in the *full range* $10^{-4} \lesssim \sin^2 2\theta_{13} \lesssim 10^{-2}$ and the third and fourth quadrants in δ_{CP} .

Note that it is dangerous to compare two configurations for only specific selected true values of $\sin^2 2\theta_{13}$ and δ_{CP} , since one can always find regions in parameter space which make this configuration appear to be very competitive. In addition, note that it may not be necessary to have a complementary experiment at all if an earlier measurement confirmed δ_{CP} be in the first or second quadrants.

Besides the technological options or alternatives, there are also physics alternatives. Within the framework of three-flavor neutrino oscillations, the most likely alternative might be a

substantial deviation from maximal mixing which would lead to the full eight-fold degeneracy [35].¹⁰ In this case, further options could be necessary to resolve this degeneracy. Depending on the parameter region, possible options include large reactor experiments or superbeams for $\sin^2 2\theta_{13} \gtrsim 10^{-2}$ [43, 95], very long baseline superbeam upgrades [96], an additional β -beam facility [91], or another neutrino factory baseline. In each of these cases, the determination of the competitive parameter space region needs further investigation.

Finally there are further reasons which justify different technologies or channels. The ν_τ appearance channel (silver channel) might, for example, be the best candidate for unitarity tests, since neutral current measurements at neutrino factories do not seem to be promising high precision measurements [97]. In the same spirit, interferences with lepton flavor violating operators [98–104], neutrino decay (see *e.g.* Ref. [105]), or other effects might lead to a different strategy.

6 Summary and conclusions

In this study, we have discussed δ_{CP} precision measurements, where we have used the concept of CP coverage as performance indicator. CP coverage represents the fraction of the remaining parameter space for δ_{CP} , *i.e.*, small values correspond to very high precisions, large values to very poor measurements, and 360° to no information on δ_{CP} at all. In comparison to CP violation measurements, the CP coverage exploits all available information on δ_{CP} . A measurement of CP violation will, for example, hardly be possible for next-generation experiments, whereas some values of δ_{CP} could already be excluded. In addition, for high precision measurements, the detection of CP violation might not be possible if the true value of δ_{CP} is close to a CP conserving value. The concept of the CP coverage carries therefore more information than a discussion of CP violation alone.

So far there exist many, very different quoted values for the precision of δ_{CP} in the literature which are based on special values of an assumed CP phase δ_{CP} . As one can see from Table 1, these different values are justified for these special values of δ_{CP} . Depending on parameter values and confidence level one can, for example, easily obtain any value between 7° (very precise measurement) and 360° (no information on δ_{CP}) for T2HK from this table. It is also apparent that there exist regularities in these values, which we have studied in this work. In particular, the strong dependence on the true value of δ_{CP} has turned out to be rather complicated, though qualitatively understandable on a quite technical level. It changes from a low-statistics (or systematics) dominated scheme to a $\sin \delta_{\text{CP}}$ -term dominated scheme (from the oscillation probabilities) as function of $\sin^2 2\theta_{13}$. In addition, there is in many cases a strong non-Gaussian dependence on the confidence level. For example, for $\sin^2 2\theta_{13} = 0.001$, $\delta_{\text{CP}} = \pi/2$, the CP coverage for NuFact-II changes more than a factor of six from the 1σ to 3σ confidence level. This non-Gaussian behavior can be understood in terms of degeneracies, which are usually not present below a certain confidence level. As an important consequence, we conclude that it does not make sense to compare the CP coverage of different experiments for selected parameter values, because one can come to almost any

¹⁰Note, however, that there has to be a substantial deviation from maximal mixing to separate the $\theta_{23} > \pi/4$ and $\theta_{23} < \pi/4$ fit regions and to change the discussion qualitatively.

Experiment/Combination	$\delta_{\text{CP}} = 0$		$\delta_{\text{CP}} = \pi/2$		$\delta_{\text{CP}} = \pi$		$\delta_{\text{CP}} = 3/2 \pi$	
$\sin^2 2\theta_{13} = 0.1$								
T2K+NO ν A+Reactor-II	90°	(360°)	108°	(360°)	96°	(360°)	145°	(300°)
T2HK	10°	(46°)	24°	(75°)	7°	(63°)	25°	(65°)
NuFact-II	38°	(133°)	47°	(131°)	28°	(99°)	46°	(132°)
$\sin^2 2\theta_{13} = 0.01$								
T2K+NO ν A+Reactor-II	259°	(360°)	232°	(360°)	360°	(360°)	187°	(360°)
T2HK	41°	(134°)	58°	(132°)	42°	(162°)	47°	(117°)
NuFact-II	24°	(74°)	31°	(94°)	11°	(40°)	39°	(101°)
$\sin^2 2\theta_{13} = 0.001$								
T2K+NO ν A+Reactor-II	360°	(360°)	360°	(360°)	360°	(360°)	296°	(360°)
T2HK	139°	(360°)	124°	(360°)	360°	(360°)	135°	(360°)
NuFact-II	27°	(141°)	17°	(111°)	23°	(93°)	30°	(133°)

Table 1: The CP coverage for different simulated values of δ_{CP} (columns) and $\sin^2 2\theta_{13}$ (row groups) for the indicated experiments or combinations of experiments. CP coverage represents the fraction of the remaining parameter space for δ_{CP} , *i.e.*, small values correspond to very high precisions, large values to very poor measurements, and 360° to no information on δ_{CP} at all. The numbers are given at the 1σ confidence level (3σ confidence level). For the other oscillation parameters, we use the standard values in this study. The definition of the assumed experimental scenarios is given in the text.

conclusion. Only a complete comparison as function of the full range of simulated values of $\sin^2 2\theta_{13}$ and δ_{CP} can support such conclusions, where the comparisons should be performed at rather high confidence levels (*e.g.*, 3σ) to include the effects of the degeneracies.

We have discussed the very complicated topology of the neutrino factory parameter space which requires the highest level of sophistication. The following major complications for the analysis and interpretation of δ_{CP} precision measurements at neutrino factories were encountered:

- The topology becomes rather flat for small values of $\sin^2 2\theta_{13}$, leading to the presence of many local minima, *i.e.*, the degeneracies are often present in complicated configurations.
- The final CP coverage depends on the relative position of the best-fit solution and $\text{sgn}(\Delta m_{31}^2)$ -degeneracy. In particular, for the true δ_{CP} in the third and fourth quadrants, the $\text{sgn}(\Delta m_{31}^2)$ -degeneracy moves as function of the simulated parameter values in the δ_{CP} fit space. This leads to complicated parameter dependencies.
- Depending on the parameter values, each of the best-fit solution and $\text{sgn}(\Delta m_{31}^2)$ -degeneracy may have a $(\delta_{\text{CP}}, \theta_{13})$ clone, which could actually double the CP coverage.

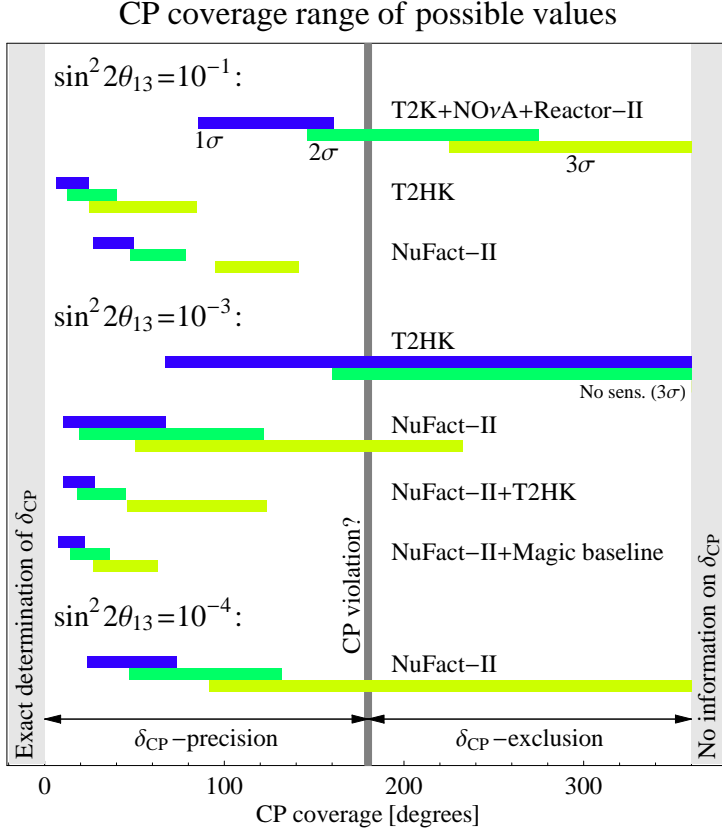


Figure 9: The ranges of possible values of the CP coverage for selected true values of $\sin^2 2\theta_{13}$ and experiments as given in the figure. The possible values of the CP coverage are given by the bands at the 1σ , 2σ , and 3σ confidence levels (from left to right). The bands therefore represent the possible outcomes of a CP precision measurements depending on the actual value of δ_{CP} , *i.e.*, they are an indicator for risk minimization of a CP precision measurement. The left half of the figure corresponds to CP precision measurements, and the right half to CP exclusion measurements, where the vertical line in the middle is a very crude estimate for CP violation capabilities (since the bands are not shown for a specific value of δ_{CP} , such as maximal CP violation $\delta_{CP} = \pi/2$).

Thus, in total, the CP coverage can vary by about a factor of four only by changing the simulated value of δ_{CP} and thus the topology of the degeneracies. Here also the strong non-Gaussian dependence on the confidence level originates.

- For large values of $\sin^2 2\theta_{13}$, neutrino factories can be highly affected by matter density uncertainties.
- Correlations *other* than with $\sin^2 2\theta_{13}$ can not be neglected. In some cases, their effect can even be as large as 100% (*cf.*, Figure 1).
- Neutrino factories contain good spectral information, which means that they can not be easily understood on the oscillation probability level.

We summarize the impact of the true value of δ_{CP} at different confidence levels for different

selected setups and simulated values of $\sin^2 2\theta_{13}$ in Figure 9. In this figure, the bands reflect the possible values of the CP coverage due to the unknown true value of δ_{CP} . This means that the CP coverage at a chosen confidence level may lay anywhere within each band. As a matter of high precision and risk minimization, one therefore wants to have the *right* edges of the bands as far left as possible. In addition, because of the non-Gaussian dependence on the confidence level in many cases, one wants to have good performances at the 3σ confidence level.

From the discussion in this study, one can finally derive a comprehensive, clean strategy to δ_{CP} precision measurements with the discussed experiments. For this purpose, we have compared the dependence on the true values of $\sin^2 2\theta_{13}$ and δ_{CP} within the full relevant ranges. The comparison as function of the true value of $\sin^2 2\theta_{13}$ has illustrated that different experiment classes clearly operate in different $\sin^2 2\theta_{13}$ regimes. The discussion as function of the true value of δ_{CP} has shown that only choosing specific values does not reflect an objective comparison. For example, choosing $\delta_{\text{CP}} = 0, \pi/2, \pi,$ and $3\pi/2$ is misleading for a neutrino factory, because its behavior is not extreme at these values (but somewhere in between). We finally conclude for δ_{CP} :

$\sin^2 2\theta_{13} \gtrsim 10^{-2}$: In this case, $\sin^2 2\theta_{13} > 0$ will be established by a reactor experiment or superbeam. As far as δ_{CP} precision is concerned, the choice to go for is a superbeam upgrade, such as T2HK. A neutrino factory is not needed in this region for a precision determination of δ_{CP} .

$\sin^2 2\theta_{13} \lesssim 10^{-2}$: For δ_{CP} precision, one wants to have a neutrino factory at a baseline of 3000 km, but with the option to add another section to the muon storage ring and a detector at a baseline of ~ 7500 km later (staged neutrino factory approach). This approach allows to first look for $\sin^2 2\theta_{13}$ down to $\sim 10^{-3}$, and check the crude value of δ_{CP} once $\sin^2 2\theta_{13} > 0$ is established. If $\sin^2 2\theta_{13}$ turns out to be smaller than $\sim 10^{-3}$ or δ_{CP} turns out to be in the third or fourth quadrants, the operation of the second “magic” baseline becomes necessary.

Note that we have not included a higher gamma β -beam in this discussion, which could, if technically feasible and competitive, replace the role of the neutrino factory. Furthermore, a substantial deviation from maximal atmospheric mixing or different physics requirements (such as unitarity tests) could require additional experiments. However, the combination between a neutrino factory and a superbeam upgrade could not be used if $\sin^2 2\theta_{13}$ turned out to be smaller than 10^{-3} . In addition, if one assumes at least one neutrino factory baseline anyway, one will from the point of view of neutrino physics have to weigh the effort of a megaton-size water Cherenkov detector (plus another accelerator facility) against the large decay tunnel slope for a second neutrino factory baseline. Therefore, one should allow for a second “magic” baseline from the beginning in the planning of a neutrino factory. This may actually not mean that one has to operate or dig the steep decay tunnel already from the beginning – one could only plan the option to do so later.

Acknowledgments

We would like to thank Steve Geer for useful discussions, which actually motivated this study. This work has been supported by SFB 375 of Deutsche Forschungsgemeinschaft and the W. M. Keck Foundation [WW].

References

- [1] M. Maltoni, T. Schwetz, M. A. Tortola, and J. W. F. Valle (2004), [hep-ph/0405172](#).
- [2] K. Anderson *et al.* (2004), [hep-ex/0402041](#).
- [3] E. Ables *et al.* (MINOS) FERMILAB-PROPOSAL-P-875.
- [4] D. Duchesneau (OPERA), eConf **C0209101**, TH09 (2002), [hep-ex/0209082](#).
- [5] P. Aprili *et al.* (ICARUS) CERN-SPSC-2002-027.
- [6] Y. Itow *et al.*, Nucl. Phys. Proc. Suppl. **111**, 146 (2001), [hep-ex/0106019](#).
- [7] D. Ayres *et al.* (2002), [hep-ex/0210005](#).
- [8] P. Zucchelli, Phys. Lett. **B532**, 166 (2002).
- [9] J. Burguet-Castell, D. Casper, J. J. Gomez-Cadenas, P. Hernandez, and F. Sanchez, Nucl. Phys. **B695**, 217 (2004), [hep-ph/0312068](#).
- [10] S. Geer, Phys. Rev. **D57**, 6989 (1998), [hep-ph/9712290](#).
- [11] M. Apollonio *et al.* (2002), [hep-ph/0210192](#).
- [12] C. Albright *et al.* (Neutrino Factory/Muon Collider) (2004), [physics/0411123](#).
- [13] V. D. Barger, K. Whisnant, and R. J. N. Phillips, Phys. Rev. Lett. **45**, 2084 (1980).
- [14] J. Arafune and J. Sato, Phys. Rev. **D55**, 1653 (1997), [hep-ph/9607437](#).
- [15] M. Tanimoto, Prog. Theor. Phys. **97**, 901 (1997), [hep-ph/9612444](#).
- [16] M. Tanimoto, Phys. Rev. **D55**, 322 (1997), [hep-ph/9605413](#).
- [17] J. Arafune, M. Koike, and J. Sato, Phys. Rev. **D56**, 3093 (1997), [hep-ph/9703351](#).
- [18] S. M. Bilenky, C. Giunti, and W. Grimus, Phys. Rev. **D58**, 033001 (1998), [hep-ph/9712537](#).
- [19] M. Koike and J. Sato (1997), [hep-ph/9707203](#).
- [20] H. Minakata and H. Nunokawa, Phys. Lett. **B413**, 369 (1997), [hep-ph/9706281](#).
- [21] H. Minakata and H. Nunokawa, Phys. Rev. **D57**, 4403 (1998), [hep-ph/9705208](#).

- [22] M. Tanimoto, Phys. Lett. **B435**, 373 (1998), [hep-ph/9806375](#).
- [23] A. De Rujula, M. B. Gavela, and P. Hernandez, Nucl. Phys. **B547**, 21 (1999), [hep-ph/9811390](#).
- [24] V. Barger, S. Geer, and K. Whisnant, Phys. Rev. **D61**, 053004 (2000), [hep-ph/9906487](#).
- [25] K. Dick, M. Freund, M. Lindner, and A. Romanino, Nucl. Phys. **B562**, 29 (1999), [hep-ph/9903308](#).
- [26] A. Donini, M. B. Gavela, P. Hernandez, and S. Rigolin, Nucl. Phys. **B574**, 23 (2000), [hep-ph/9909254](#).
- [27] M. Freund, M. Lindner, S. T. Petcov, and A. Romanino, Nucl. Phys. **B578**, 27 (2000), [hep-ph/9912457](#).
- [28] M. Koike and J. Sato, Phys. Rev. **D61**, 073012 (2000), [hep-ph/9909469](#).
- [29] A. Romanino, Nucl. Phys. **B574**, 675 (2000), [hep-ph/9909425](#).
- [30] J. Sato, Nucl. Instrum. Meth. **A451**, 36 (2000), [hep-ph/9910442](#).
- [31] A. Cervera *et al.*, Nucl. Phys. **B579**, 17 (2000), [hep-ph/0002108](#).
- [32] H. Minakata and H. Nunokawa, Nucl. Instrum. Meth. **A472**, 421 (2000), [hep-ph/0009091](#).
- [33] H. Minakata and H. Nunokawa, Phys. Lett. **B495**, 369 (2000), [hep-ph/0004114](#).
- [34] M. Koike, T. Ota, and J. Sato, Nucl. Phys. **B615**, 331, [hep-ph/0011387](#).
- [35] V. Barger, D. Marfatia, and K. Whisnant, Phys. Rev. **D65**, 073023 (2002), [hep-ph/0112119](#).
- [36] A. Bueno, M. Campanelli, S. Navas-Concha, and A. Rubbia, Nucl. Phys. **B631**, 239 (2002), [hep-ph/0112297](#).
- [37] J. Burguet-Castell, M. B. Gavela, J. J. Gomez-Cadenas, P. Hernandez, and O. Mena, Nucl. Phys. **B608**, 301 (2001), [hep-ph/0103258](#).
- [38] M. Koike, T. Ota, and J. Sato, Phys. Rev. **D65**, 053015, [hep-ph/0103024](#).
- [39] H. Minakata and H. Nunokawa, Nucl. Instrum. Meth. **A503**, 218 (2001), [hep-ph/0111130](#).
- [40] J. Pinney and O. Yasuda, Phys. Rev. **D64**, 093008 (2001), [hep-ph/0105087](#).
- [41] M. Aoki, K. Hagiwara, and N. Okamura, Phys. Lett. **B554**, 121 (2003), [hep-ph/0208223](#).

- [42] V. Barger, D. Marfatia, and K. Whisnant, Phys. Lett. **B560**, 75 (2003), [hep-ph/0210428](#).
- [43] J. Burguet-Castell, M. B. Gavela, J. J. Gomez-Cadenas, P. Hernandez, and O. Mena, Nucl. Phys. **B646**, 301 (2002), [hep-ph/0207080](#).
- [44] A. Donini, D. Meloni, and P. Migliozi, Nucl. Phys. **B646**, 321 (2002), [hep-ph/0206034](#).
- [45] P. Huber, M. Lindner, and W. Winter, Nucl. Phys. **B645**, 3 (2002), [hep-ph/0204352](#).
- [46] P. Huber, M. Lindner, and W. Winter, Nucl. Phys. **B654**, 3 (2003), [hep-ph/0211300](#).
- [47] H. Minakata, H. Nunokawa, and S. Parke (2002), [hep-ph/0208163](#).
- [48] H. Minakata, H. Nunokawa, and S. J. Parke, Phys. Lett. **B537**, 249 (2002), [hep-ph/0204171](#).
- [49] T. Ota and J. Sato (2002), [hep-ph/0211095](#).
- [50] K. Whisnant, J. M. Yang, and B.-L. Young, Phys. Rev. **D67**, 013004 (2003), [hep-ph/0208193](#).
- [51] D. Autiero *et al.* (2003), [hep-ph/0305185](#).
- [52] B. Brahmachari, S. Choubey, and P. Roy, Nucl. Phys. **B671**, 483 (2003), [hep-ph/0303078](#).
- [53] M. V. Diwan *et al.* (2003), [hep-ph/0303081](#).
- [54] A. Donini, D. Meloni, and S. Rigolin, JHEP **06**, 011 (2004), [hep-ph/0312072](#).
- [55] P. Huber and W. Winter, Phys. Rev. **D68**, 037301 (2003), [hep-ph/0301257](#).
- [56] M. Mezzetto, J. Phys. **G29**, 1771 (2003), [hep-ex/0302007](#).
- [57] P. Migliozi and F. Terranova, Phys. Lett. **B563**, 73 (2003), [hep-ph/0302274](#).
- [58] H. Minakata and H. Sugiyama, Phys. Lett. **B580**, 216 (2004), [hep-ph/0309323](#).
- [59] T. Ohlsson and W. Winter, Phys. Rev. **D68**, 073007 (2003), [hep-ph/0307178](#).
- [60] L.-Y. Shan *et al.*, Phys. Rev. **D68**, 013002 (2003), [hep-ph/0303112](#).
- [61] W. Winter, Phys. Rev. **D70**, 033006 (2004), [hep-ph/0310307](#).
- [62] M. Blom and H. Minakata, New J. Phys. **6**, 130 (2004), [hep-ph/0404142](#).
- [63] P. Huber, M. Lindner, M. Rolinec, T. Schwetz, and W. Winter, Phys. Rev. **D70**, 073014 (2004), [hep-ph/0403068](#).
- [64] O. Mena and S. Parke, Phys. Rev. **D70**, 093011 (2004), [hep-ph/0408070](#).

- [65] H. Minakata (2004), [hep-ph/0402197](#).
- [66] I. Ambats *et al.* (NOvA) FERMILAB-PROPOSAL-0929.
- [67] M. Freund, Phys. Rev. **D64**, 053003 (2001), [hep-ph/0103300](#).
- [68] E. K. Akhmedov, R. Johansson, M. Lindner, T. Ohlsson, and T. Schwetz (2004), [hep-ph/0402175](#).
- [69] J. N. Bahcall, M. C. Gonzalez-Garcia, and C. Pena-Garay, JHEP **08**, 016 (2004), [hep-ph/0406294](#).
- [70] A. Bandyopadhyay, S. Choubey, S. Goswami, S. T. Petcov, and D. P. Roy (2004), [hep-ph/0406328](#).
- [71] M. Maltoni, T. Schwetz, M. A. Tortola, and J. W. F. Valle, Phys. Rev. **D68**, 113010 (2003), [hep-ph/0309130](#).
- [72] H. Minakata and H. Nunokawa, JHEP **10**, 001 (2001), [hep-ph/0108085](#).
- [73] G. L. Fogli and E. Lisi, Phys. Rev. **D54**, 3667 (1996), [hep-ph/9604415](#).
- [74] P. Lipari, Phys. Rev. **D61**, 113004 (2000), [hep-ph/9903481](#).
- [75] P. Huber, J. Phys. **G29**, 1853 (2003), [hep-ph/0210140](#).
- [76] G. L. Fogli, E. Lisi, A. Marrone, and D. Montanino, Phys. Rev. **D67**, 093006 (2003), [hep-ph/0303064](#).
- [77] R. J. Geller and T. Hara, Phys. Rev. Lett. **49**, 98 (2001), [hep-ph/0111342](#).
- [78] S. V. Panasyuk, *Rem (reference earth model) web page* (2000), <http://cfauvcs5.harvard.edu/lana/rem/index.htm>.
- [79] P. Huber, M. Lindner, and W. Winter (2004), <http://www.ph.tum.de/~globes>, [hep-ph/0407333](#).
- [80] M. C. Gonzalez-Garcia and C. Peña-Garay, Phys. Lett. **B527**, 199 (2002), [hep-ph/0111432](#).
- [81] V. D. Barger, D. Marfatia, and B. P. Wood, Phys. Lett. **B498**, 53 (2001), [hep-ph/0011251](#).
- [82] P. Huber, M. Lindner, T. Schwetz, and W. Winter, Nucl. Phys. **B665**, 487 (2003), [hep-ph/0303232](#).
- [83] P. Huber, M. Lindner, M. Rolinec, and W. Winter, in preparation.
- [84] W. Winter, AIP Conf. Proc. **721**, 227 (2004), [hep-ph/0308227](#).
- [85] D. Beavis *et al.*, *Proposal of BNL AGS E-889*, Tech. Rep., BNL (1995).

- [86] H. Minakata, H. Nunokawa, and S. J. Parke, Phys. Rev. **D68**, 013010 (2003), [hep-ph/0301210](#).
- [87] H. Minakata, H. Sugiyama, O. Yasuda, K. Inoue, and F. Suekane, Phys. Rev. **D68**, 033017 (2003), [hep-ph/0211111](#).
- [88] Y. F. Wang, K. Whisnant, Z.-h. Xiong, J. M. Yang, and B.-L. Young (VLBL Study Group H2B-4), Phys. Rev. **D65**, 073021 (2002), [hep-ph/0111317](#).
- [89] V. Barger, D. Marfatia, and K. Whisnant, Phys. Rev. **D66**, 053007 (2002), [hep-ph/0206038](#).
- [90] A. Asratyan *et al.*, Science **124**, 103 (2003), [hep-ex/0303023](#).
- [91] A. Donini, E. Fernandez-Martinez, P. Migliozzi, S. Rigolin, and L. Scotto Lavina (2004), [hep-ph/0406132](#).
- [92] O. Yasuda (2004), [hep-ph/0405005](#).
- [93] A. Donini, E. Fernandez-Martinez, and S. Rigolin (2004), [hep-ph/0411402](#).
- [94] J. Bouchez, M. Lindroos, and M. Mezzetto (2003), [hep-ex/0310059](#).
- [95] K. B. McConnell and M. H. Shaevitz (2004), [hep-ex/0409028](#).
- [96] M. V. Diwan (2004), [hep-ex/0407047](#).
- [97] V. Barger, S. Geer, and K. Whisnant (2004), [hep-ph/0407140](#).
- [98] L. M. Johnson and D. W. McKay, Phys. Rev. **D61**, 113007 (2000), [hep-ph/9909355](#).
- [99] A. M. Gago, M. M. Guzzo, H. Nunokawa, W. J. C. Teves, and R. Zukanovich Funchal, Phys. Rev. **D64**, 073003 (2001), [hep-ph/0105196](#).
- [100] M. C. Gonzalez-Garcia, Y. Grossman, A. Gusso, and Y. Nir, Phys. Rev. **D64**, 096006 (2001), [hep-ph/0105159](#).
- [101] P. Huber, T. Schwetz, and J. W. F. Valle, Phys. Rev. Lett. **88**, 101804 (2002), [hep-ph/0111224](#).
- [102] T. Ota, J. Sato, and N.-a. Yamashita, Phys. Rev. **D65**, 093015 (2002), [hep-ph/0112329](#).
- [103] P. Huber, T. Schwetz, and J. W. F. Valle, Phys. Rev. **D66**, 013006 (2002), [hep-ph/0202048](#).
- [104] T. Ota and J. Sato (2004), [hep-ph/0410408](#).
- [105] M. Lindner, T. Ohlsson, and W. Winter, Nucl. Phys. **B607**, 326 (2001), [hep-ph/0103170](#).